Holocene sea ice history and climate variability along the main axis of the Northwest Passage, Canadian Arctic

David Ledu,[1,2] André Rochon,[1,2] Anne de Vernal,[2] Francesco Barletta,[1,2] and Guillaume St-Onge[1,2]

Received 21 June 2009; revised 13 December 2009; accepted 7 January 2010; published 18 June 2010.

[1] Palynological, geochemical, and physical records were used to document Holocene paleoceanographic changes in marine sediment core from Dease Strait in the western part of the main axis of the Northwest Passage (core 2005-804-006 PC latitude 68°59.552′N, longitude 106°34.413′W). Quantitative estimates of past sea surface conditions were inferred from the modern analog technique applied to dinoflagellate cyst assemblages. The chronology of core 2005-804-006 PC is based on a combined use of the paleomagnetic secular variation records and the CALS7K.2 time-varying spherical harmonic model of the geomagnetic field. The age-depth model indicates that the core spans the last ~7700 cal years B.P., with a sedimentation rate of 61 cm ka^{-1}. The reconstructed sea surface parameters were compared with those from Barrow Strait and Lancaster Sound (cores 2005-804-004 PC and 2004-804-009 PC, respectively), which allowed us to draw a millennial-scale Holocene sea ice history along the main axis of the Northwest Passage (MANWP). Overall, our data are in good agreement with previous studies based on bowhead whale remains. However, dinoflagellate sea surface based reconstructions suggest several new features. The presence of dinoflagellate cysts in the three cores for most of the Holocene indicates that the MANWP was partially ice-free over the last 10,000 years. This suggests that the recent warming observed in the MANWP could be part of the natural climate variability at the millennial time scale, whereas anthropogenic forcing could have accelerated the warming over the past decades. We associate Holocene climate variability in the MANWP with a large-scale atmospheric pattern, such as the Arctic Oscillation, which may have operated since the early Holocene. In addition to a large-scale pattern, more local conditions such as coastal current, tidal effects, or ice cap proximity may have played a role on the regional sea ice cover. These findings highlight the need to further develop regional investigations in the Arctic to provide realistic boundary conditions for climatic simulations.

Citation: Ledu, D., A. Rochon, A. de Vernal, F. Barletta, and G. St-Onge (2010), Holocene sea ice history and climate variability along the main axis of the Northwest Passage, Canadian Arctic, *Paleoceanography*, *25*, PA2213, doi:10.1029/2009PA001817.

1. Introduction

[2] Major hydrographical changes took place in the Arctic over the past few decades. The decline of sea ice cover extent, which began in the late 1970s, has accelerated since 1998 reaching a historical record low in the summer of 2007 [*Comiso et al.*, 2008; *Deser and Teng*, 2008; *Stroeve et al.*, 2008]. This minimum was 25% lower than the previous summer 2005 record and 40% lower than the 1979–2006 average based on satellite measurements [*Schweiger et al.*, 2008]. This reduction in sea ice has occurred mainly in the western sector of the Arctic Ocean and on the Russian shelves. Satellite-derived summer mean sea surface temperature (SST) anomalies since 2000 reveal warm anomalies during 2002–2005 over the Bering Strait, the Beaufort and the eastern Siberian seas [*Steele et al.*, 2008]. This "Arctic warm period" [*Overland et al.*, 2008] has been mostly associated with changes in the atmospheric circulation identified as the Northern Annular Mode (NAM), also known as the Arctic Oscillation (AO) [*Thompson and Wallace*, 1998]. The AO creates a marked SST and sea ice dipole pattern between the eastern and western Arctic [*Rigor et al.*, 2002; *Vavrus and Harrison*, 2003; *Zhang et al.*, 2003]. Dinoflagellate cyst assemblages in cores from the Labrador Sea [*de Vernal et al.*, 2001], Baffin Bay and Hudson Strait [*Levac et al.*, 2001; *Rochon et al.*, 2006] suggest a reduced sea ice cover during the early Holocene, whereas cores from the Beaufort and Chukchi seas indicate a steady decrease of sea ice cover from the early to late Holocene [*de Vernal et al.*, 2005a; *Rochon et al.*, 2006; *McKay et al.*, 2008]. Similarly, *Ledu et al.* [2008a, 2008b, also Holocene paleoceanography of the Northwest Passage, Canadian Arctic Archipelago, submitted to *Quaternary Science Reviews*, 2010] reconstructed an opposite trend between the easternmost (Lancaster Sound) and central (Barrow Strait) part of the MANWP during the same interval.

[1]ISMER, UQAR, Rimouski, Quebec, Canada.
[2]GEOTOP, Université du Québec à Montréal, Montreal, Quebec, Canada.

0883-8305/10/2009PA001817

[3] The main objective of this paper is to better understand the spatial character of this dipolar structure in the Arctic Ocean, i.e., to spatially define the east–west thermal gradient, and to better understand the mechanism(s) behind its potential variability at the millennial time scale. For this purpose, marine sediment cores in the westernmost (Dease Strait), central (Barrow Strait) and easternmost (Lancaster Sound) part of the MANWP were collected during the ArcticNet oceanographic campaigns of summer 2004 and 2005. Due to their strong relationship with sea surface parameters in the Arctic and subarctic seas [*de Vernal et al.* 2001, 2005b; *de Vernal and Marret*, 2007], their relatively high species diversity and good preservation in polar sediments [*Kokinos et al.*, 1998; *de Vernal et al.*, 2001], organic-walled dinoflagellate cysts also known as dinocysts, were used as tracer of past sea surface conditions. Quantitative estimates of the duration of sea ice cover (months/year) as well as summer sea surface temperature (SSTs) and salinity (SSSs) were derived from the modern analog technique [*de Vernal et al.*, 2001, 2005b]. This method yields one of the lowest root mean square error of prediction (RMSEP) among transfer functions techniques [*Guiot and de Vernal*, 2007]. Here we present the new results from Dease Strait and we compare sea surface reconstructions with those from cores recovered from Barrow Strait and Lancaster Sound [*Ledu et al.*, 2008a, also submitted manuscript].

2. Environmental Setting

[4] The MANWP connects the eastern and western Arctic across the Canadian Arctic Archipelago (CAA), which is one of the largest continental shelves in the Arctic Ocean [*Jakobsson*, 2002]. About 70% of the channels in the CAA are shallower than 500 m depth except toward the eastern side of Barrow Strait. The mean depth in the western part of the MANWP was estimated at ~125 m [*Jakobsson*, 2002; *McLaughlin et al.*, 2004]. As a consequence, the water column is strongly influenced by Pacific water origin [*Jones et al.*, 2003] derived from the Canada Basin through Amundsen Gulf and M'Clure Strait. This flow is strongly associated with the Beaufort Gyre (BG) and the transpolar drift (TPD), which both contribute to sea ice and freshwater export from the western to the eastern Arctic. Typically, the upper 40–50 m of the water column is occupied by a cold low salinity mixed layer (ML), which is influenced in summer by sea ice melt, river plume spreading and by brine rejection during sea ice f ormation in winter. The upper halocline (between 40 and 50 m and 125 m) is composed of summer Pacific water including both the relatively warm and fresh Alaskan Coastal Current water (ACCW, $31<S<32$ and $1°C<T°<6°C$) and the relatively colder and saltier summer Bering Seawater (sBSW, $32<S<33$ and $0°C<T°<2°C$). The middle and lower halocline (between 125 and 200 m) are composed of the winter Bering Seawater (wBSW) near the freezing point with salinity ranging from 32.5 to 33.1. The respective importance and mixing of these water masses varies in time and space within the Canada Basin [*Steele et al.*, 2004]. In the northern BG, the ACCW overlains the summer Bering Seawater, which flows above the winter Bering Seawater. In contrast, in the southern BG the ACCW overlies the wBSW [*Steele et al.*, 2004]. The warm (up to 3°C) and salty (~34.5) intermediate Atlantic water flows between 200 and 800 m [*Shimada et al.*, 2001; *McLaughlin et al.*, 2004]. Below 800 m, only the deep water masses of Atlantic origin are found [*Carmack et al.*, 2008]. It has been shown that both the low salinity water content of the Canada Basin and its export into the CAA as well as the flux from the CAA to the North Atlantic Ocean were strongly influenced by the Beaufort gyre (BG) and the transpolar drift (TPD), which are strongly dependent of the AO mode [*Proshutinsky et al.* 2002; *Steele et al.*, 2004; *Prinsenberg and Hamilton*, 2005]. Instrumental data reveal that the AO has operated at annual to decadal time scales over the past 40 years across the Arctic Ocean [*Polyakov and Johnson*, 2000; *Venegas and Mysak*, 2000; *Dukhovskoy et al.*, 2004; *Polyakov et al.*, 2004]. Recent studies suggest that it could have operated since the early Holocene [*Darby and Bischof*, 2004; *de Vernal et al.*, 2005a; *McKay et al.*, 2008; *Ledu et al.*, 2008a, also submitted manuscript; *Fréchette and de Vernal*, 2009]. Although the chronological resolution of Holocene sedimentary records in the Arctic, generally does not permit inference on annual to decadal frequency of positive and negative AO modes, it may serve to document what was the dominant mode at the centennial to millennial time scales.

3. Materials and Methods

3.1. Coring Site and Sampling

[5] Sampling in the MANWP was carried out in the summers of 2004 and 2005, during leg 9 and leg 1 of the ArcticNet oceanographic campaigns aboard the CCGS *Amundsen*. The sampling sites were selected using a Simrad EM 300 multibeam echo sounder and a Simrad 3.5 kHz subbottom profiler to avoid disturbed sediment areas (i.e., erosion, mudflows and/or mass movements). Cores from Dease Strait, Barrow Strait and Lancaster Sound were collected using a piston corer (hereinafter, referred to as cores 006 PC, 004 PC and 009 PC, respectively (for details see Table 1 and Figure 1)). Box cores (BC) and trigger weight cores (TWC) were also collected at each site. Palynological analyses for core 009 and 004 BC can be found in previous studies (for details see *Ledu et al.* [2008a, 2008b, also submitted manuscript]). Here, BC and TWC were used to estimate top piston core sediment missing due to piston coring process (see section 4.1 and Figure 2). Sampling for palynological analyses was performed at a 10 cm sampling interval and each subsample was then processed according to the standard palynological preparation technique described by *Rochon et al.* [1999]. The taxonomy of dinocysts used in this work conforms to that of *Rochon et al.* [1999], *de Vernal et al.* [2001] and *Head et al.* [2001].

3.2. Quantitative Estimates of Past Sea Surface Conditions

[6] Quantitative estimates of past sea surface conditions were made using the modern analog technique (MAT) and the software R. MAT was applied to dinocyst assemblages following the procedures described by *de Vernal et al.* [2005b]. The method consists of comparing fossil assem-

Table 1. Geographic Coordinates of the Coring Sites in Dease Strait, Barrow Strait, and Lancaster Sound[a]

Core ID	Latitude N	Longitude W	Length of the Core (cm)	Water Depth (m)
2005-804-006 PC	68°59.552′	106°34.413′	400	118
2005-804-004 PC	74°16.155′	91°05.48′	670	350
2004-804-009 PC	74°11.2′	81°11.7′	600	781

[a]Core 2005-804-006 PC is in Dease Strait, core 2005-804-004 PC is in Barrow Strait, and core 2004-804-009 PC is in Lancaster Sound.

blage samples with modern assemblages from a reference database. Here, we used the updated reference dinocyst database, which includes 64 taxa and 1189 sites from the North Atlantic, North Pacific, Arctic Ocean and subpolar seas [*de Vernal et al.*, 2005b; *Radi and de Vernal*, 2008]. The distance or degree of dissimilarity between the fossil spectrum to be analyzed and the spectra in the reference database is calculated after logarithmic transformation of percentage data. The modern spectra with the lowest distance then permit identifying the best modern analogs. Here, we used a set of five modern analogs from which hydrographic parameters (SSTs and SSSs and the duration of sea ice cover expressed as the number of months per year with sea ice concentration greater than 50%) were averaged after weighting inversely to the distance of the analogs. This average constitutes the most probable estimates. The hydrographic data are compiled using the 2001 version of the World Ocean Atlas [*National Oceanography Data Center* (*NODC*), 2001], in addition to the duration of sea ice cover which is derived from the 1953–2000 data set provided by *National Snow and Ice Data Center* (*NSIDC*) [1953–2000], in Boulder, Colorado.

[7] Quantitative estimates of sea surface conditions using MAT yields good results as indicated by coefficients of correlation greater than 0.93 between estimated and instru-

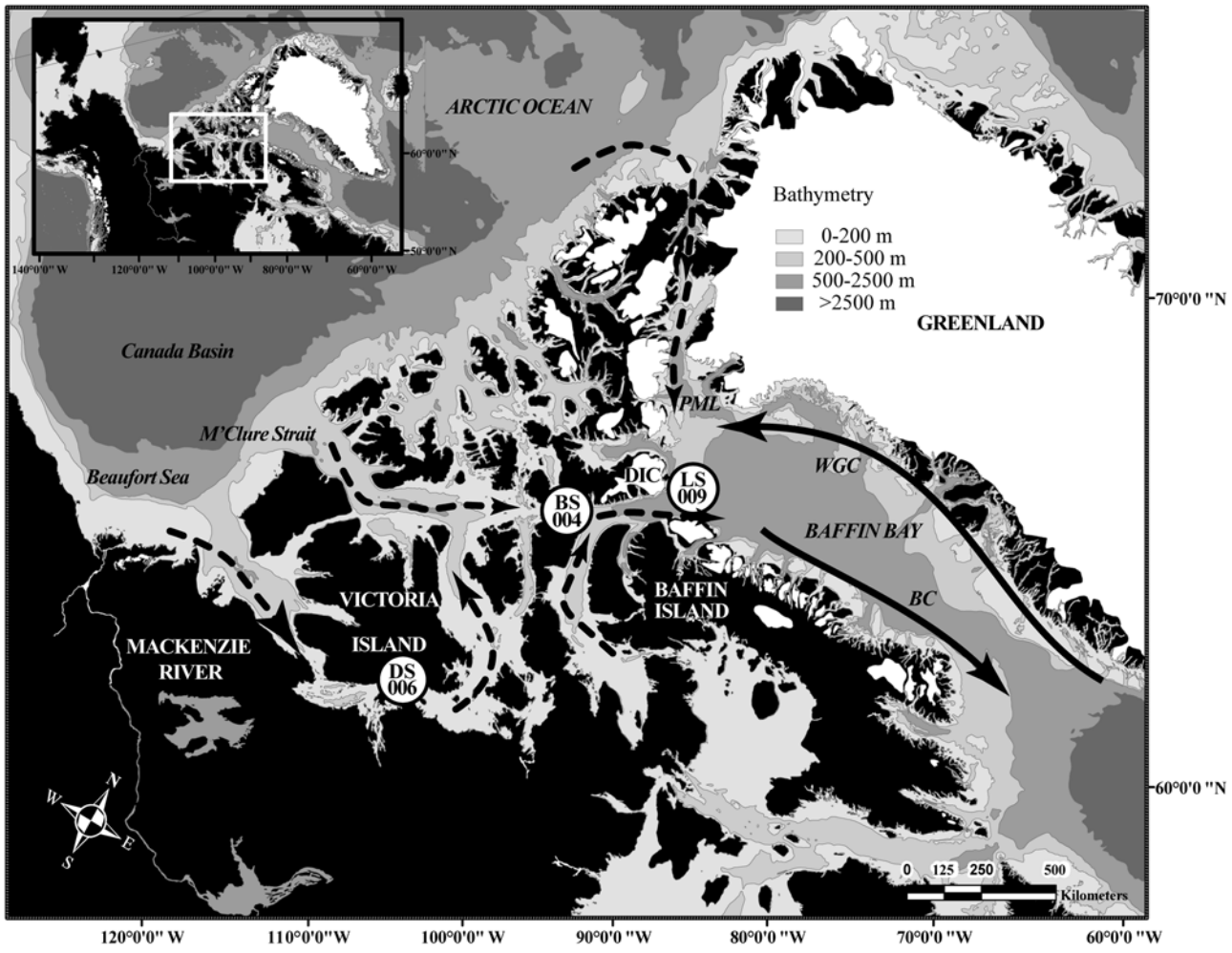

Figure 1. Location of the coring sites (white circles) at Dease Strait (DS 006), Barrow Strait (BS 004), and Lancaster Sound (LS 009) with major surface currents in the CAA. Modern ice caps are also shown (white coverage (DIC, Devon Island ice cap)). The circulation in the CAA has an eastward component. Dashed black arrows correspond to the Polar Mixed Layer whereas the solid black arrows correspond to the Atlantic water (BC, Baffin Current; WGC, West Greenland Current; PML, Polar Mixed Layer).

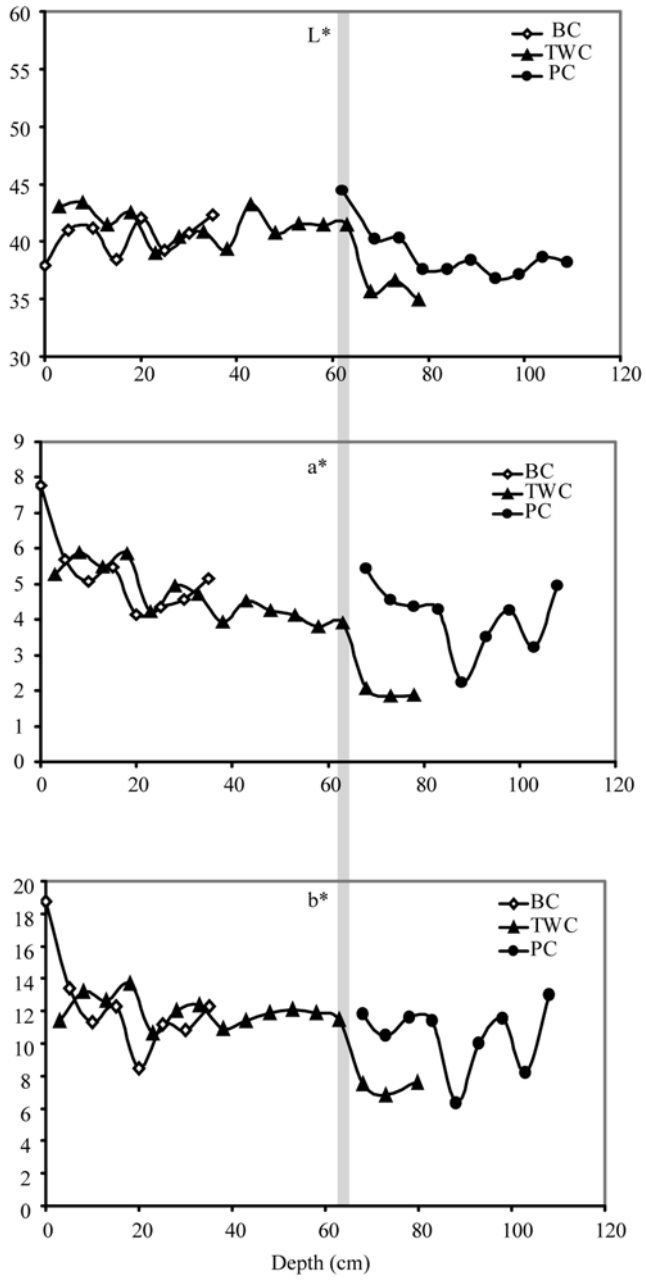

Figure 2. Diagrams showing the color reflectance (L*a*b*) for cores 006 BC, TWC, and PC, used here to estimate top piston core sediment missing due to piston coring process (see text for details). The gray line indicates that about 63 cm of sediment from core 006 PC was lost during coring process. Note that only the upper 110 cm of core 006 PC is shown.

mental hydrographic parameters. The degree of accuracy of the estimated reconstructions is obtained by the calculation of the standard deviation of the residual (estimated minus observed values), which is ± 1.5°C for the SSTs, ± 1.8 for the SSSs and ± 1.1 months/year for the duration of sea ice cover. Modern conditions in Dease Strait are 8.5 ± 1.3 months/year for the sea ice cover, 3.9 ± 2°C and 25 ± 3 for the August SSTs and SSSs, respectively [*NSIDC*, 1953–2000; *NODC*, 2001].

3.3. Carbon and Nitrogen Stable Isotopes

[8] Total carbon (C_{Total}) and total nitrogen N_{Total} content were measured using Carlo-Erba elemental analyzer at the Geochemistry and Geodynamics Research Center (GEOTOP), Montréal. The carbon isotopic composition of organic matter ($\delta^{13}C_{org}$) was measured by continuous-flow mass spectrometry using a Carlo-Erba elemental analyzer connected to an Isoprime mass spectrometer. It is expressed in standard notation δ versus Vienna Peedee belemnite (VPDB). The error, which is based on replicate analyses, is ± 0.004% for N, ± 0.015% for C and ± 0.1‰ for the $\delta^{13}C_{org}$.

3.4. Color Reflectance

[9] Diffuse spectral reflectance was measured with a X-Rite digital swatchbook DTP-22 handheld spectrophotometer on board the CCGS *Amundsen*. Reflectance data were then converted in the L*a*b* color space. High values (low values) of L* indicate white (black) color, whereas positive (negative) values of a* indicate red (green) and positive (negative) values of b* correspond to yellow (blue). The L*a*b* data were used to estimate missing sediment due to the piston coring process (Figure 2).

3.5. Grain Size and Paleomagnetic Measurements

[10] Grain size measurements (fraction between 0.04 – 2000 μm) were performed at the Institut des sciences de la mer de Rimouski (ISMER) using a Beckman-Coulter LS 13320 laser diffraction grain size analyzer. Grain size distribution and statistical parameters (mean and standard deviations) were derived from the Gradistat software [*Blott and Pye*, 2001]. The whole core low field volumetric magnetic susceptibility (k_{LF}) of the sediment was determined at 2 cm intervals using a GEOTEK multi sensor core logger (MSCL) on board the CCGS *Amundsen*. k_{LF}, depends mainly to the concentration of ferromagnetic minerals (e.g., magnetite) but is also grain size dependent [e.g., *Dunlop and Özdemir*, 1997]. The natural remanent magnetization (NRM) was measured at the Sedimentary Paleomagnetism Laboratory at ISMER, using a 2G Enterprises Model SRM-755 cryogenic magnetometer on u channels (rigid u-shaped plastic liners with a 2 cm square cross section and a length of ~1.5 m) at 1 cm intervals. However, due to the finite spatial resolution of the magnetometer's pickup coils, each measurement integrates a stratigraphic interval of 5 cm [*Weeks et al.*, 1993]. In order to eliminate this edge effect, the data from the upper and lower 5 cm of each u channel were excluded. To isolate the characteristic remanent magnetization (ChRM), the NRM was measured and progressively demagnetized applying peak alternative fields (AF) of 0 to 80 mT at 5 mT increments. The component inclination of the ChRM (ChRM I) was calculated using a least squares line fitting procedure [*Kirschvink*, 1980]. In addition, the precision of the best fit procedure was estimated by the maximum angular deviation (MAD). Last, the median destructive field of the NRM (MDF_{NRM}, the value of the peak AF field necessary to

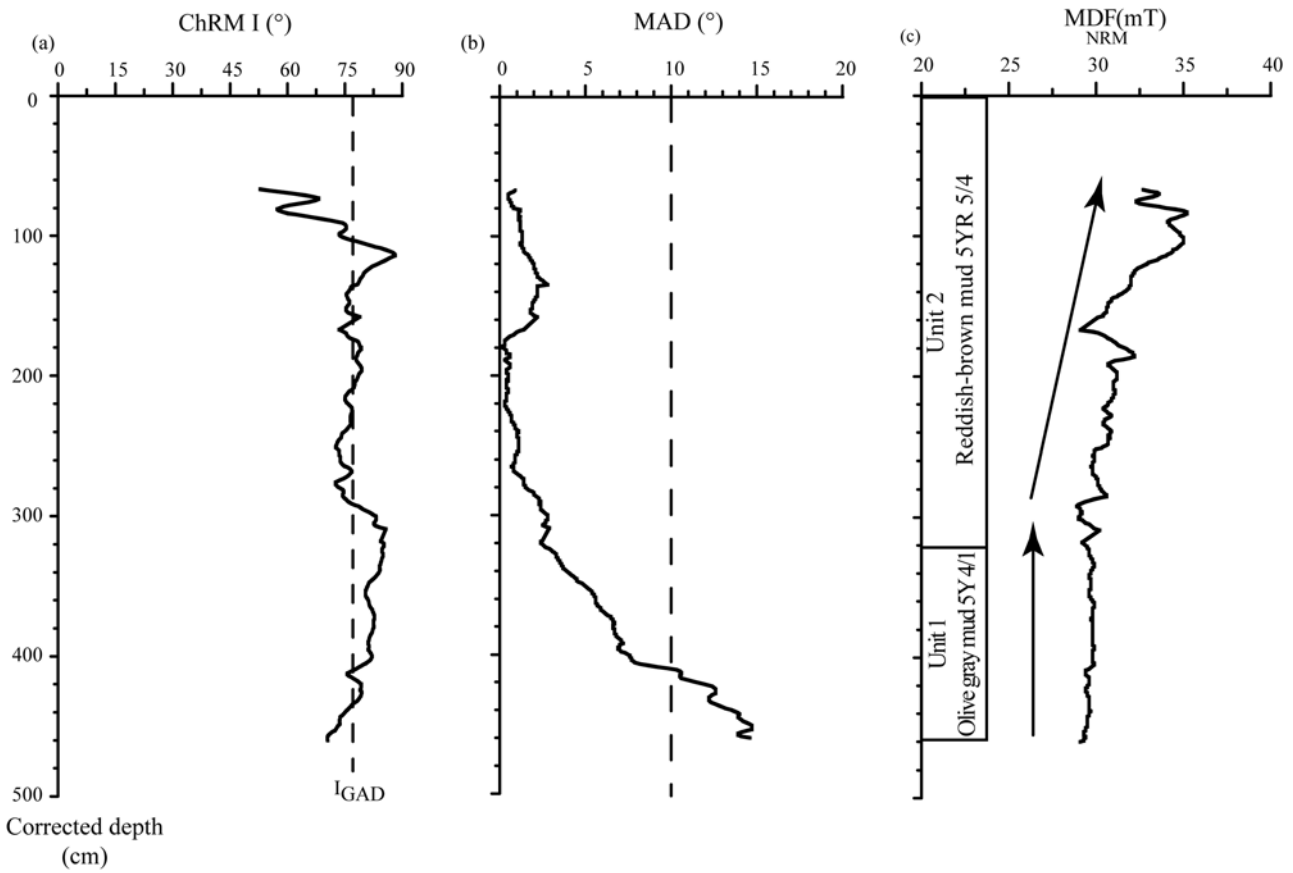

Figure 3. (a and b) Diagrams showing the ChRM I and the MAD values for core 006 PC. The vertical dashed line is the value of the geocentric axial dipole (GAD) for the ChRM I at Dease Strait site. (c) Diagram showing the median destructive field of the NRM (MDF_{NRM}; see text for details) and the lithological units of core 006 PC. Note the two distinct trends in the MDF_{NRM} parameter (as indicated by arrows) associated with the gradual change in color sediment (colors are given according to the Munsell soil color charts).

reduce the NRM intensity to half of its initial value) was derived in order to characterize changes in magnetic grain size and mineralogy.

3.6. Chronology of the Cores

[11] In the study core, biogenic carbonate was too rare for accelerator mass spectrometry (AMS) ^{14}C measurements and the chronostratigraphy is based on geomagnetic directional changes, also known as paleomagnetic secular variations (PSV). Arctic Holocene magnetic inclination and declination profiles have been correlated from distant as well as proximate sites [*Lund*, 1996; *Stoner et al.*, 2007; *Barletta et al.*, 2008a, 2008b; *Besonen et al.*, 2008; *Lisé-Pronovost et al.*, 2009; Ledu et al., submitted manuscript]. Significant Holocene geomagnetic directional changes have been documented in high latitude environments (Baffin Bay, central Finland, northern Sweden, St Lawrence Estuary, Siberia, Russia, Fennoscandia, Iceland, Beaufort and Chukchi seas, Canadian Arctic and Alaskan margins, main axis of the Northwest Passage [e.g., *Andrews and Jennings*, 1990; *Saarinen*, 1998; *Snowball and Sandgren*, 2002; *St-Onge et al.*, 2003; *Korte and Constable*, 2005; *Snowball et al.*, 2007; *Stoner et al.*, 2007; *Barletta et al.*, 2008a; *Besonen et al.*, 2008, *Lisé-Pronovost et al.*, 2009; Ledu et al., submitted manuscript]). These PSV records have been used as a relative dating method [*Saarinen*, 1999; *Kotilainen et al.*, 2000; *St-Onge et al.*, 2003, 2004; *Breckenridge et al.*, 2004; *Stoner et al.*, 2007; *Barletta et al.*, 2008b; *Lisé-Pronovost et al.*, 2009; Ledu et al., submitted manuscript]. Recently, *Barletta et al.* [2008b], *Lisé-Pronovost et al.* [2009] and Ledu et al. (submitted manuscript) found a strong consistency between the Holocene inclination data in cores from the Chukchi and Beaufort seas, the Alaskan margin, the MANWP and the calculated inclination using the CALS7K.2 time-varying spherical harmonic model of *Korte and Constable* [2005]. Due to their proximity to the North Magnetic Pole, cores from high latitudes have the potential to record higher amplitude directional changes, which are well represented by the CALS7K.2 model at the millennial to centennial time scale [*Barletta et al.*, 2008a; *Lisé-Pronovost et al.*, 2009; Ledu et al., submitted manuscript].

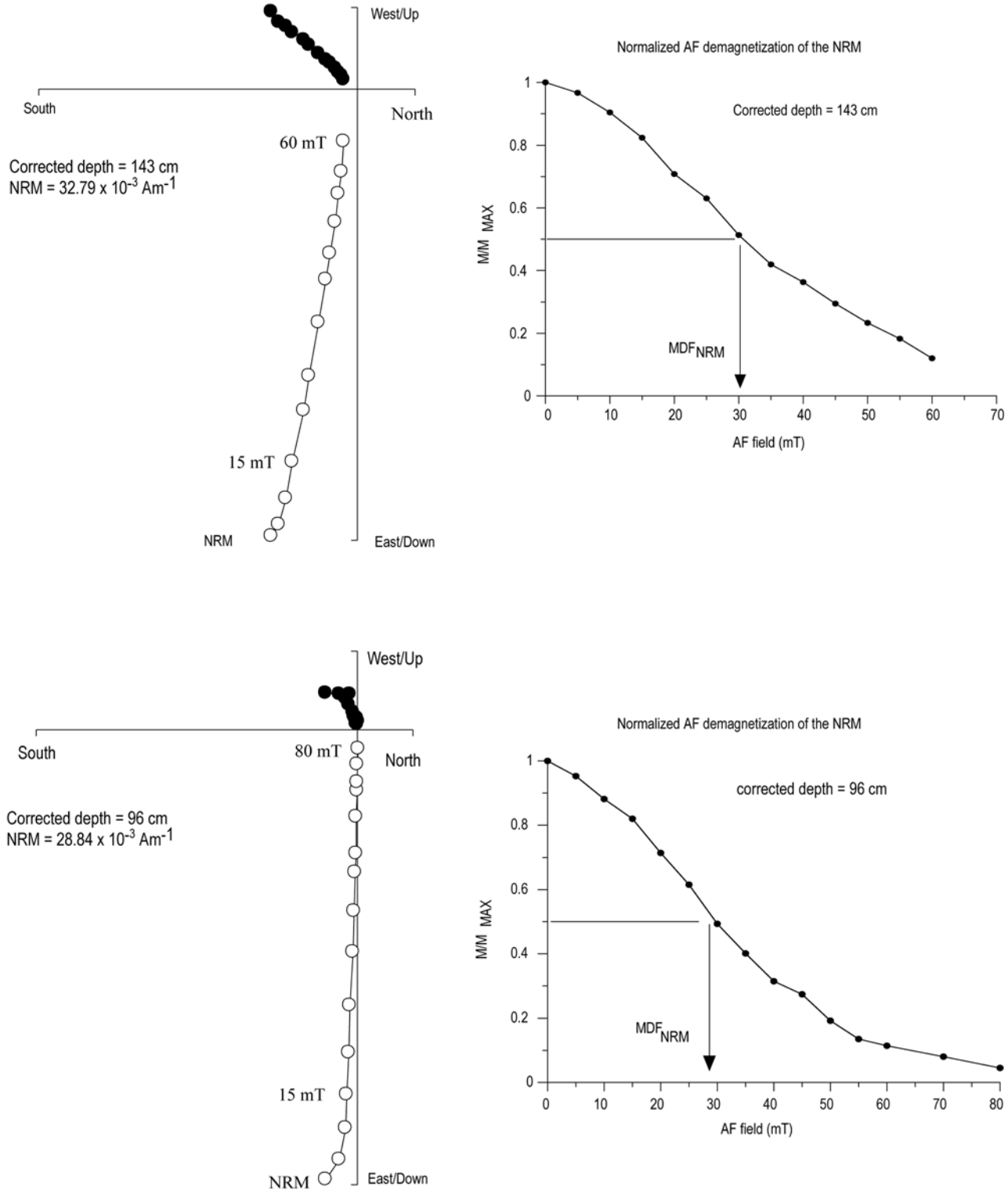

Figure 4. (left) Typical vector end point orthogonal projection diagrams [*Zijderveld*, 1967] at two selected depths. Solid data points indicate vector end points projected onto the horizontal plane, open data points indicate vector end points projected onto the vertical plane, and numbers adjacent to data points are the AF demagnetization steps. (right) The normalized AF demagnetization curves for the NRM are shown. At the 60 mT AF demagnetization step, only ~10% of the initial NRM is still present, supporting the absence of high-coercivity magnetic components.

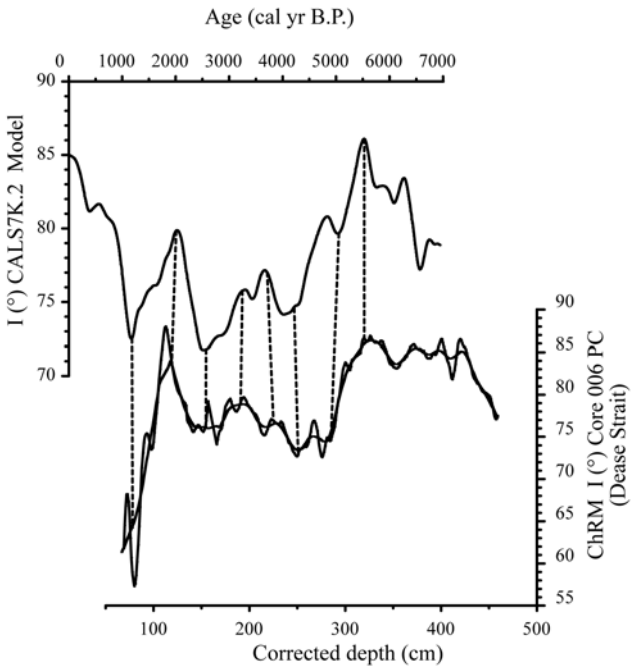

Figure 5. ChRM I for core 006 PC and magnetic inclination I (°) for Dease Strait inferred from the CALS7K.2 model. The dashed lines are the suggested correlations with the CALS7K.2 model [*Korte and Constable*, 2005].

[12] Here, we present a chronology for core 006 PC based on the combined used of PSV records (here the magnetic inclination) and the CALS7K.2 model [*Korte and Constable*, 2005].

4. Results

4.1. Lithological Description and Missing Sediment

[13] Core 006 PC is composed of two lithological units (see Figure 3). The first unit between 463 and 323 cm (from ca 7730 to 5400 cal years B.P.) consists of olive gray mud (5Y 4/1, Munsell color chart) and is overlained by the second unit between 323 cm and the top (ca 5400 to 1000 cal years B.P.) of the core, which consists of reddish brown mud (5YR 5/4). Variable degree of bioturbation appears along the entire core but it is mostly developed in the second lithological unit. The comparison based on the L*a*b* color space between the trigger weight (TWC) and the piston cores (PC) indicate that about 63 cm was lost during the coring process (Figure 2). Note that all depths of core 006 PC are expressed in corrected depth, which account for the missing sediment.

4.2. Paleomagnetic Secular Variation Records and Composite Age-Depth Model

[14] The AF demagnetization behavior of the NRM of core 006 PC reveals the presence of two magnetic components: a low-coercivity magnetic component (viscous magnetization) easily removed in the 0–15 mT AF range and a stable, well-defined, magnetic component in the 20–80 mT AF range (Figure 3). Aside from the last 50 cm where the ChRM is less well defined (MAD > 10°), MAD values are generally lower than 5° while the ChRM I fluctuate around the expected inclination value for a geocentric axial dipole model (I_{GAD} = 77° [e.g., *Butler*, 1992]). Assuming a relatively uniform magnetic grain-size assemblage variations in the downcore MDF_{NRM} parameters are generally ascribed to change in the coercivity of the magnetic minerals [e.g., *Stoner and St-Onge*, 2007]. As revealed in Figure 3, the transitional change in color sediment is clearly associated with an increase of the MDF_{NRM}. In addition, red minerals are often associated with the presence of high-coercivity minerals (i.e., titanohematites [*Dunlop and Özdemir*, 1997]). Accordingly, variations in the MDF_{NRM} profile are probably due to change in magnetic mineralogy. According to *Stoner and St-Onge* [2007] titanomagnetites are the primary remanence carrier for high-quality PSV records. It is possible that high-coercivity minerals could affect the quality of the PSV record (i.e., the ChRM I). However, as revealed by the analysis of the Zijderveld diagrams (Figure 4), an extremely stable and well-defined (MAD < 5°) magnetic component in the low to medium coercivity spectrum has been isolated. Based on these results, a possible effect of high-coercivity mineral(s) on the PSV record is negligible.

[15] Furthermore, the MDF_{NRM} varies between 28.9 and 35.2 mT supporting the presence of a low-coercivity ferrimagnetic mineral (most likely magnetite) as principal carrier of the isolated ChRM (Figure 4). Accordingly, the magnetic properties of core 006 PC meet all the criteria necessary to have a reliable PSV record [e.g., *Stoner and St-Onge*, 2007].

[16] Using the predicted magnetic inclination for our coring site over the last 7000 cal years B.P. computed from the CALS7K.2 model and the magnetic inclination of core 006 PC, we constructed an age-depth relationship based on 8 paleomagnetic tie points that result from the comparison of both records (Figure 5 and Table 2a). The age-depth model was constructed using a linear fit between ages on a composite depth scale corrected for missing sediment due to the piston coring process (Figures 2 and 6). In order to test the reliability of our age-depth model, we compared the magnetic inclination record of core 006 PC based on its new chronology with other Holocene PSV records from the western Canadian Arctic [*Barletta et al.*, 2008a; *Lisé-Pronovost et al.*, 2009], and the western northern America

Table 2a. Paleomagnetic Tie Points Used to Construct the Age-Depth Relationship for Core 006 PC[a]

CALS7K.2 Age (cal yr B.P.)	Depths Equivalence[b] (cm)
1200	63
2000	117
2530	155
3265	190
3655	225
4100	250
5000	280
5500	325

[a]See text for details about constructing the age-depth relationship.
[b]Depths equivalence are based on PSV correlation. Note that all the depths equivalence are expressed in a corrected depth, which accounts for missing sediment due to piston coring processes (see text for details).

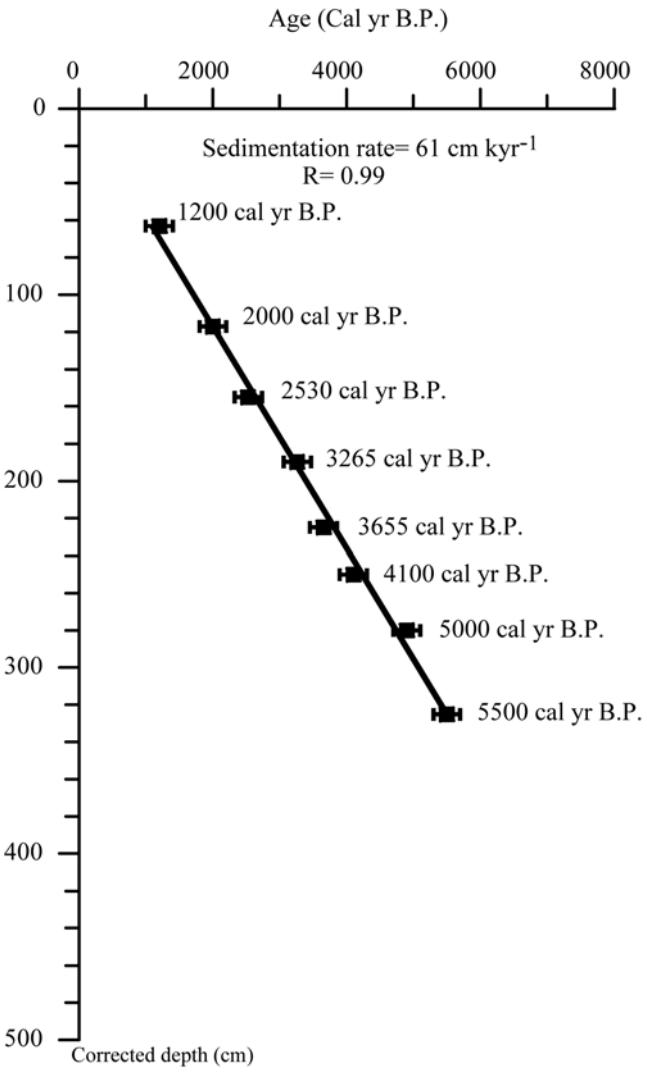

Figure 6. Age-depth model for core 006 PC based on correlations between PSV records (ChRM I) and the CALS7K.2 predicted inclination for Dease Strait. A linear fit was used to construct the age depth relationship (R = 0.99). An error bar of ± 200 years has been assigned to each age on the age-depth profile, which accounts for both the temporal resolution uncertainty of the CALS7K.2 model and the error associated with the linear fit as well as the lock-in process related to the post depositional remanent magnetization (for details see *Stoner and St-Onge* [2007]).

(Fish Lake, Oregon, USA [*Verosub et al.*, 1986]). Major shifts of the magnetic inclination are observed in all cores around 1000, 2000, 2500, 3500, 4500 and 5500 cal years B.P. and are on average 150 ± 40 years from those recorded in core 006 PC (Figure 7a). Theses shifts are also well recorded by the CALS7K.2 model output and all paleomagnetic inclination records indicate a shallowing trend between ~6000 and ~2500 cal years B.P. (Figure 7a). The age-depth model indicates that core 006 PC spans the last 7730 cal years B.P., with a constant sedimentation rate of 61 cm ka^{-1} (Figure 6). Chronologies for cores 009 PC and 004 PC are also based on a composite record between the magnetic inclination and the predicted inclination for both sites derived from the CALS7K.2 (background data set; Figure 7b) (Ledu et al. submitted manuscript). The age depth models indicate that core 009 PC and 004 PC span approximately the last 11,000 years. The calculated sedimentation rates range from 43 to 140 cm ka^{-1} and from 15 to 118 cm ka^{-1} for cores 009 and 004 PC, respectively (background data set; Figure 7b and Table 2b). Based on these sedimentation rates and the sampling interval, we can achieve a centennial to millennial time scale resolution (background data set; Table 2b).

4.3. Grain Size and Stable Isotopes

[17] Grain size analyses (Figure 8) show the dominant silt (more than 75%) and clay fractions. Geochemical data (Figure 8) indicate that carbon and nitrogen content are relatively constant along the core, except in the lower part, between 6000 and 5000 cal years B.P. During this interval, the organic carbon content (C_{org}) records its highest values (1.63%, core average 0.8%), whereas the inorganic carbon content (C_{inorg}) and $CaCO_3$ display there lowest values (0.2% and 1.6%, core average 1.05% and 9%, respectively). This is accompanied by high value of the C/N ratio (22, core average 9.8) and low value of the $\delta^{13}C_{org}$ content (−23.9‰, core average −23.1‰ versus VPDB).

4.4. Dinocyst Assemblages and Reconstruction of Sea Surface Parameters

[18] Well-preserved dinocyst are present throughout the core, with concentrations ranging from 950 to 10,930 cysts/cm^3 (mean 1935 cysts/cm^3) and maximum values reached between 6000 and 5500 cal years B.P. (Figure 9). This corresponds to fluxes of 667 cysts/cm^2 $year^{-1}$, which most likely reflect a high productivity. The ratio of phototrophic to heterotrophic dinocyst taxa (Gonyaulacales (G)/Peridiniales (P), G/P ratio) records values ranging from 0.03 to 0.66 (mean 0.32) indicating the dominance of heterotrophic taxa although photosynthetic taxa occur in significant number. It is noticeable that the relative abundance of the heterotrophic taxon *Brigantedinium* spp. is higher than 50% throughout the core. Its maximum abundance in the Canadian Arctic has been associated with the Mackenzie freshwater plume in the Beaufort Sea or more generally with nutrient-rich area [*Mudie and Rochon*, 2001; *Richerol et al.*, 2008a, 2008b] or polynyas [*Hamel et al.*, 2002].

[19] Based on the relative abundance of dinocyst taxa, core 006 PC shows three different zones (Figure 9). The first zone, between 7730 and ~6000 cal years B.P. is dominated by the heterotrophic taxa *Brigantedinium* spp. (~75%), *Islandinium minutum* (5–10%), and the phototrophic taxon *Operculodinium centrocarpum* (~15–20%). Quantitative estimates of past sea surface conditions suggest a sea ice cover slightly above modern conditions (up to 1 month/year) with SSTs (August) that fluctuate around modern values but with a general decreasing trend. Minimum SSTs (August, 1°C) is reached around 6500 cal years B.P., which is 2.5°C cooler compared to modern conditions. This is accompanied by a general increase in SSSs (August).

[20] The second zone between 6000 and 3000 cal years B.P. is also characterized by the dominance of *Brigantedinium*

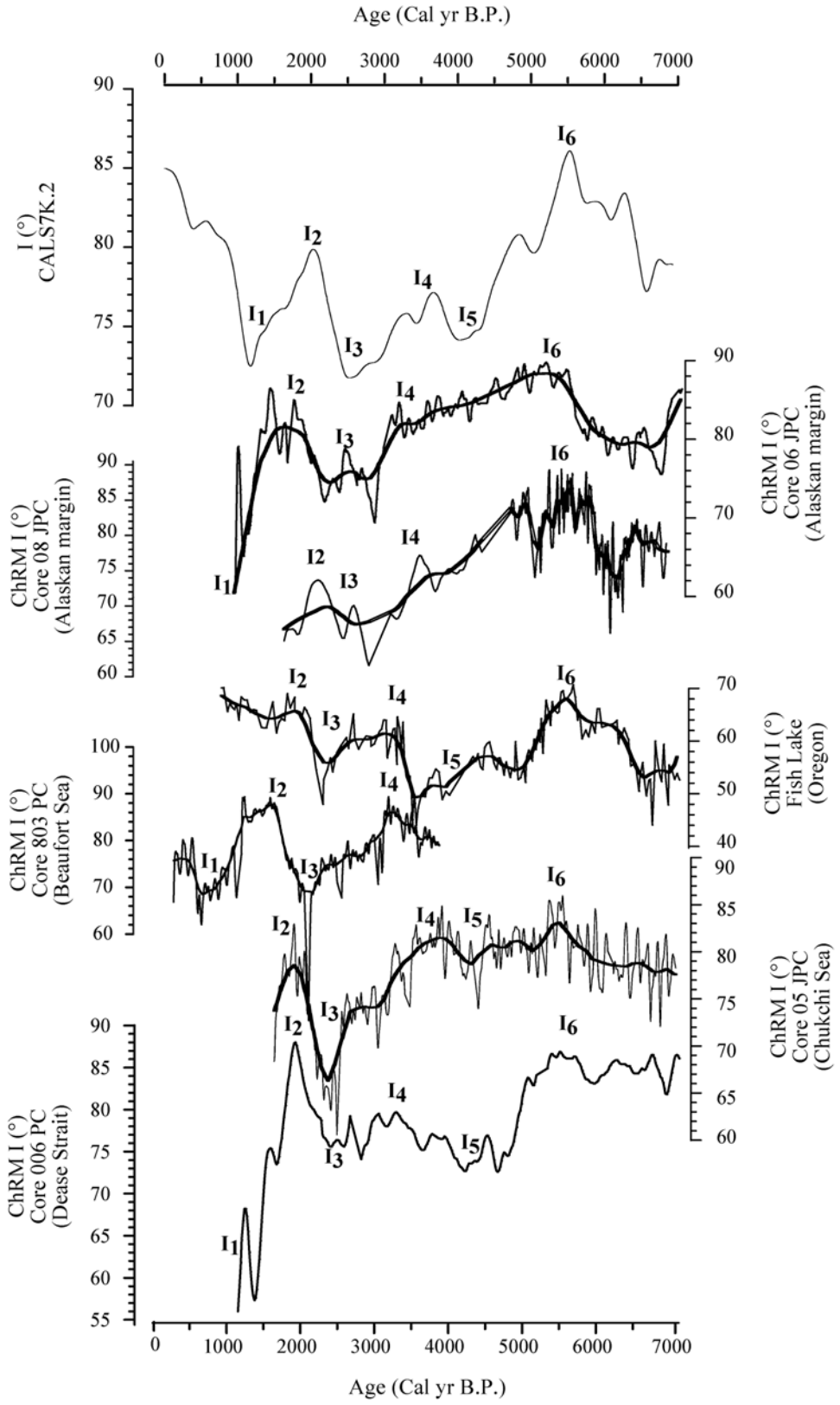
Age (Cal yr B.P.)
0 1000 2000 3000 4000 5000 6000 7000
I (°)
CALS7K.2
ChRM I (°)
Core 08 JPC
(Alaskan margin)
ChRM I (°)
Core 06 JPC
(Alaskan margin)
ChRM I (°)
Core 803 PC
(Beaufort Sea)
ChRM I (°)
Fish Lake
(Oregon)
ChRM I (°)
Core 006 PC
(Dease Strait)
ChRM I (°)
Core 05 JPC
(Chukchi Sea)
I1
I2
I3
I4
I5
I6

Figure 7a

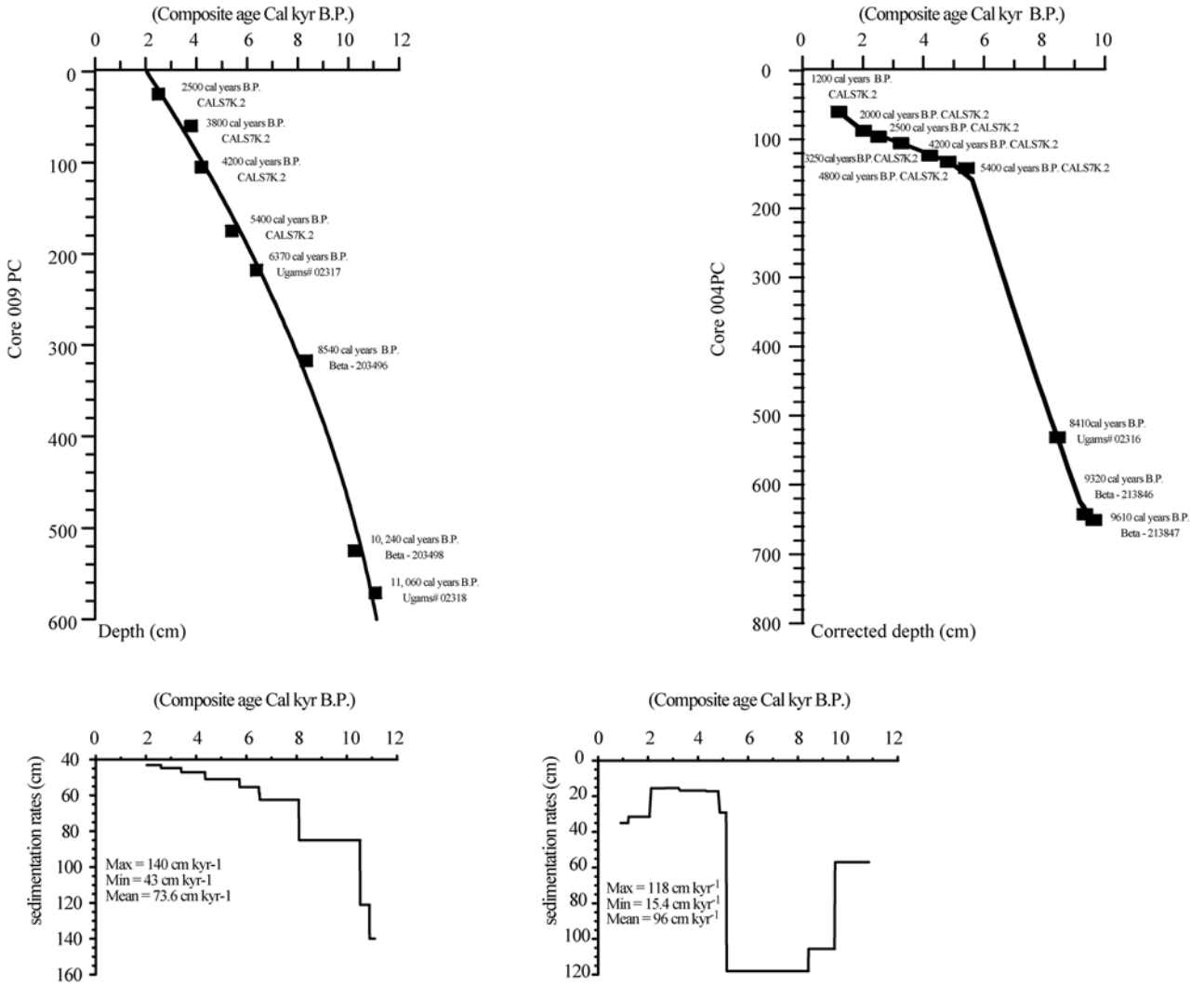

Figure 7b. Background data set. (top) Composite age model for cores 009 and 004 PC based on correlations between PSV records (ChRM I) and the CALS7K.2 predicted inclination for both sites with initial AMS-^{14}C ages (see text and Table 2a for details). The age model is based on a second-order polynomial fit for core 009 PC and a linear interpolation fit for core 004 PC. (bottom) Sedimentation rates as suggested by the age models (modified from Ledu et al. (submitted manuscript)).

spp. (more than 50%) and *Operculodinium centrocarpum* (~25%) but it is marked by the occurrence of the phototrophic taxon *Pentapharsodinium dalei* and of the heterotrophic taxon *Selenophemphix quanta*. These are also marked by an increase in the relative abundance of *Islandinium minutum* var. *cezare* and the maximum abundance of the cyst of *Polykrikos* arctic morphotype. The reconstructed SSTs and SSSs (August) fluctuate around modern conditions. Maximum SSTs (August) are reached at ~5500, 5200 and 4000 cal years B.P. and corresponds to an increase of 2.5°C with regards to modern conditions whereas minimum values are reached around 4700 cal years B.P. (2.5°C lower

Figure 7a. Comparison of the ChRM I between core 006 PC and other cores from the Chukchi and Beaufort seas [*Barletta et al.*, 2008a], North America (Fish Lake, Oregon [*Verosub et al.*, 1986]), and the Alaskan margin [*Lisé-Pronovost et al.*, 2009]. Core 006 PC is on its new composite chronology (see text for details). The top diagram corresponds to the CALS7K.2 model of the predicted magnetic inclination for Dease Strait [*Korte and Constable*, 2005]. Major ChRM I shifts observed in all records occurred around 1000 (I_1), 2000 (I_2), 2500 (I_3), 3500 (I_4), 4500 (I_5), and 5500 (I_6) cal years B.P. Note the shallow magnetic inclination, which is marked in all records between 6000 and 2500 cal years B.P.

Table 2b. Sedimentation Rates, Sampling Interval, and Time Scale Resolutions for Cores 009, 004, and 006 PC[a]

Time Interval (cal yr B.P.)	Sedimentation Rates (cm ka^{-1})	Sampling Interval (cm)	Time Resolutions (year)
	2004-804-009 PC		
2,034–2,590	43.1	10	232
2,590–3,394	44.8	-	223
3,416–4,348	47.1	-	212
4,369–5,720	51	-	196
5,740–6,495	55.4	-	180
6,512–6,530	58.8	-	170
6,547–8,082	62.4	-	160
8,097–10,528	85	-	117
10,537–10,906	121	-	82
10,913–11,113	140	-	71
	2005-804-004 PC		
914–1,200	35	-	285
1,228–2,059	31.4	-	318
2,123–2,640	15.5	-	645
2,704–3,220	15.4	-	649
3,285–4,292	16.8	-	595
4,350–4,815	17.2	-	581
4,873–5,123	29.2	-	342
5,152–8,419	118	-	84
8,427–9,470	105.6	-	94
9,488–10,831	57	-	175
	2005-804-006 PC		
1,023–7,730	61	-	166

[a]Background data set.

than modern). Sea ice cover is rather stable and similar to that of the first zone.

[21] The third zone, between 3000 and 1000 cal years B.P. is marked by both the gradual increase dominance of *Brigantedinium* spp. and the gradual decrease in the relative abundance of *Operculodinum centrocarpum*. In the uppermost part of the zone, the relative abundance of *Brigantedinium* spp. reaches 88%, whereas that of *Operculodinium centrocarpum* is around 10%. These are also accompanied by the disappearance of *Selenopemphix quanta* and *Spiniferites elongatus/frigidus*. Quantitative estimates of past sea surface parameters indicate a general cooling trend with minimum values of 0°C in August at 1500 and 1000 cal years B.P., which is 3.5°C lower than modern conditions. The cooling trend is accompanied by SSSs (August) and sea ice cover increase. Maximum sea ice cover is reached at 1500 and 1000 cal years B.P. with values ~1.5 months/year more than present conditions.

4.5. Other Palynomorph Concentrations

[22] Other organic-walled microfossils show relatively low concentrations throughout the length of core. However, between 6000 and 5500 cal years B.P., core 006 PC depicts a strong increase of the pollen, spores, brackish water algae *Halodinium*, pre-Quaternary reworked palynomorphs and organic linings of foraminifers (OL) concentrations (Figure 10). Maximum values are reached during that time with pollen concentration of 605 grains/cm^3 (average 79 grains/cm^3) and spores concentration of 213 individuals/cm^3 (average 30 spores/cm^3). Pre-Quaternary reworked palynomorphs (average 48 individuals/cm^3), *Halodinium* (average 213 individuals/cm^3), and organic linings of foraminifers (average 234 individuals/cm^3) also indicate maximum concentration with values of 533, 213, 1601 individuals/cm^3, respectively. The pollen/dinocyst ratio (P/D ratio, average 0.04) shows a slight increase during that time (from 0.02 to 0.05).

5. Discussion

5.1. Early Middle Holocene in the Main Axis of the Northwest Passage

[23] Quantitative estimates of past sea surface conditions (Figures 9 and 11) suggest relatively harsh conditions in

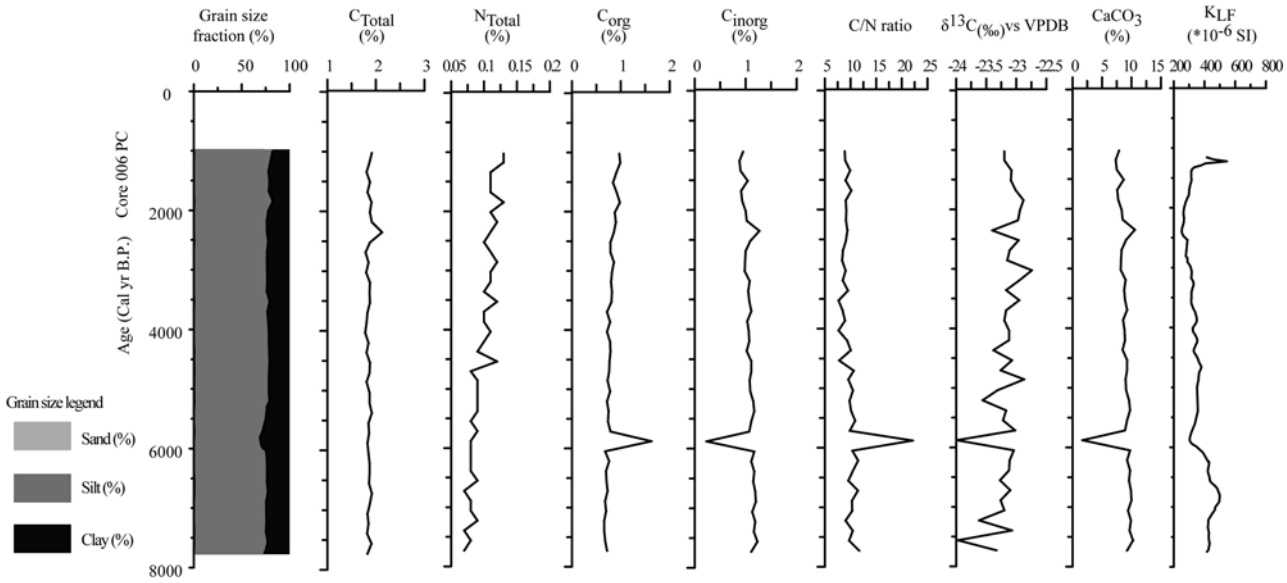

Figure 8. Grain size, carbon, and nitrogen stable isotopes content of core 006 PC. The magnetic susceptibility is also shown.

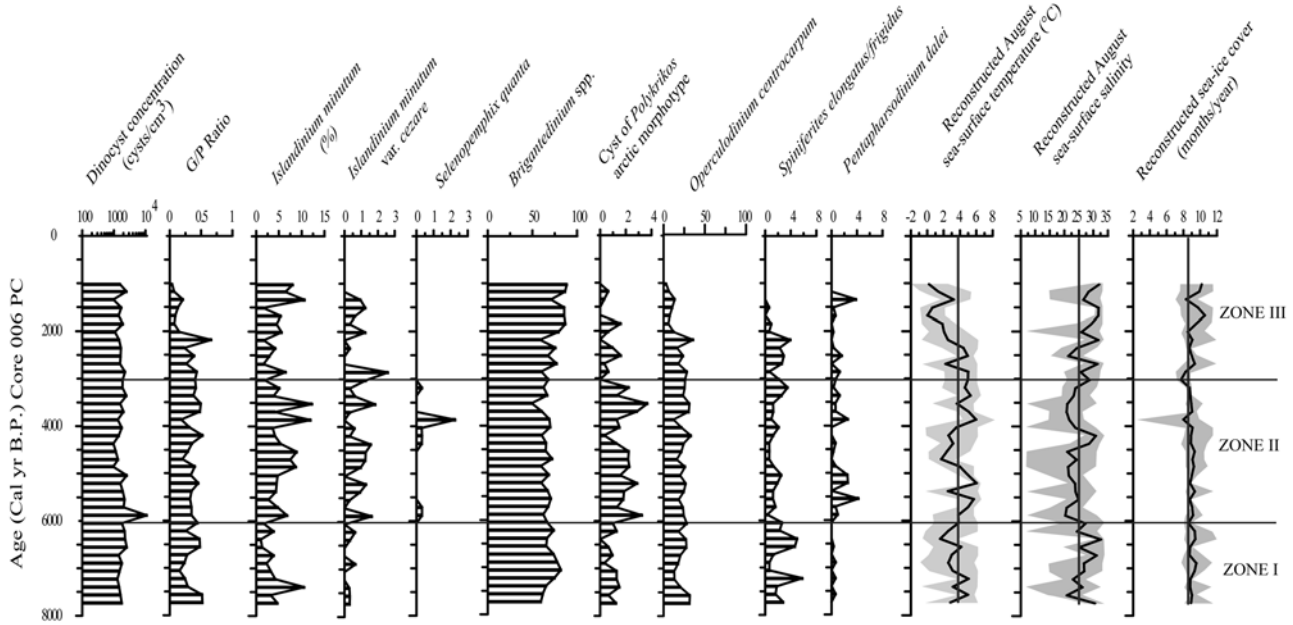

Figure 9. Diagram of dinocyst concentration, Gonyaulacales/Peridiniales (G/P ratio), relative abundance of dinocyst taxa, and quantitative estimates of sea surface conditions based on modern analog technique (MAT) applied to dinocyst assemblages in core 006 PC. The thick black lines correspond to the best estimates, which are the averages weighted inversely to the distance for the five best modern analogs. The gray zones correspond to the minimum and maximum values possible according to the set of five best analogs. The vertical gray lines indicate the values of modern sea surface conditions, and the horizontal gray lines are the different zones based on dinocyst assemblages (see text for details).

Dease Strait during the early to middle Holocene (from ca 7730 to 6000 cal years B.P.). It corresponds to the zone I, where the reconstructed SSTs (August) are relatively low (2.5°C lower than modern conditions around 6500 cal years B.P.). This is accompanied by little sea ice change with respect to modern conditions and a general increase of the reconstructed SSSs (August, maximum of 32 reached around 6500 cal years B.P.). Similarly, paleoceanographic records based on dinocyst assemblages in core 004 PC (Barrow Strait; Figure 11) also indicate low SSTs (August, on average 1°C, modern conditions 1.9°C) with sea ice cover, which fluctuates around present conditions (maximum of 11.3 months/year, minimum of 9 months/year, present conditions of 10.2 months/year). Records based on dinocyst assemblages, mesopelagic and benthic foraminifers from the Chukchi Sea [*McKay et al.*, 2008; *de Vernal et al.*, 2005a] also indicate relatively harsh conditions with a sharp halocline promoting an extensive sea ice cover. These differ from marine records from the eastern Arctic, which rather indicate warmer conditions in the early middle Holocene. Dinocyst assemblages in core 009 PC (Lancaster Sound; Figure 11), and from northernmost Baffin Bay indicate an increase in the relative abundance of phototrophic taxa beginning around 8500 cal years B.P., accompanied by a general trend toward warmer SSTs [*Levac et al.*, 2001; *Rochon et al.*, 2006; *Ledu et al.*, 2008b, also submitted manuscript]. Maximum SST was also found from sites along or near the North Atlantic Current and its components from the early to middle Holocene [*de Vernal and Hillaire-Marcel*, 2006]. These are consistent with a maximum inflow of Atlantic water recorded by mesopelagic and benthic foraminifers in cores from the Barents Sea, Chukchi Sea, west Greenland, Svalbard and Iceland shelves around 8000 cal years B.P. [*Hillaire-Marcel et al.*, 2004; *de Vernal et al.*, 2005a; *Duplessy et al.*, 2005; *Lloyd et al.*, 2005; *Ślubowska-Woldengen et al.*, 2008].

[24] In modern conditions, the positive mode of the AO creates such climatic conditions in the Arctic [*Dickson et al.*, 2000; *Rigor et al.*, 2002; *Zhang et al.*, 2003]. These include an increase advection of Atlantic water into the Arctic Ocean with strong divergence in the eastern Arctic resulting in positive SST anomalies, whereas convergence in the western Arctic enhanced negative SST anomalies accompanied by an extensive sea ice cover, but with little variations [*Rigor et al.*, 2002; *Zhang et al.*, 2003]. A more northward position of the jet stream enhanced an increase of Eurasian river discharge with a more eastward component along the East Siberian seas and the Canada Basin [*Peterson et al.*, 2002; *Schlosser et al.*, 2002; *Steele et al.*, 2004]. These processes create a negative sea surface salinity anomaly in most of the Canada Basin [*Steele and Ermold*, 2004], which enhances a strong stratification promoting the formation of sea ice. Therefore, we associate the relatively harsh conditions in the westernmost/central (Dease/Barrow Straits) as well as the milder conditions in the easternmost part of the MANWP (Lancaster Sound) with a positive mode of the AO. In the eastern Arctic, this was accompanied by major oceanographic changes, including

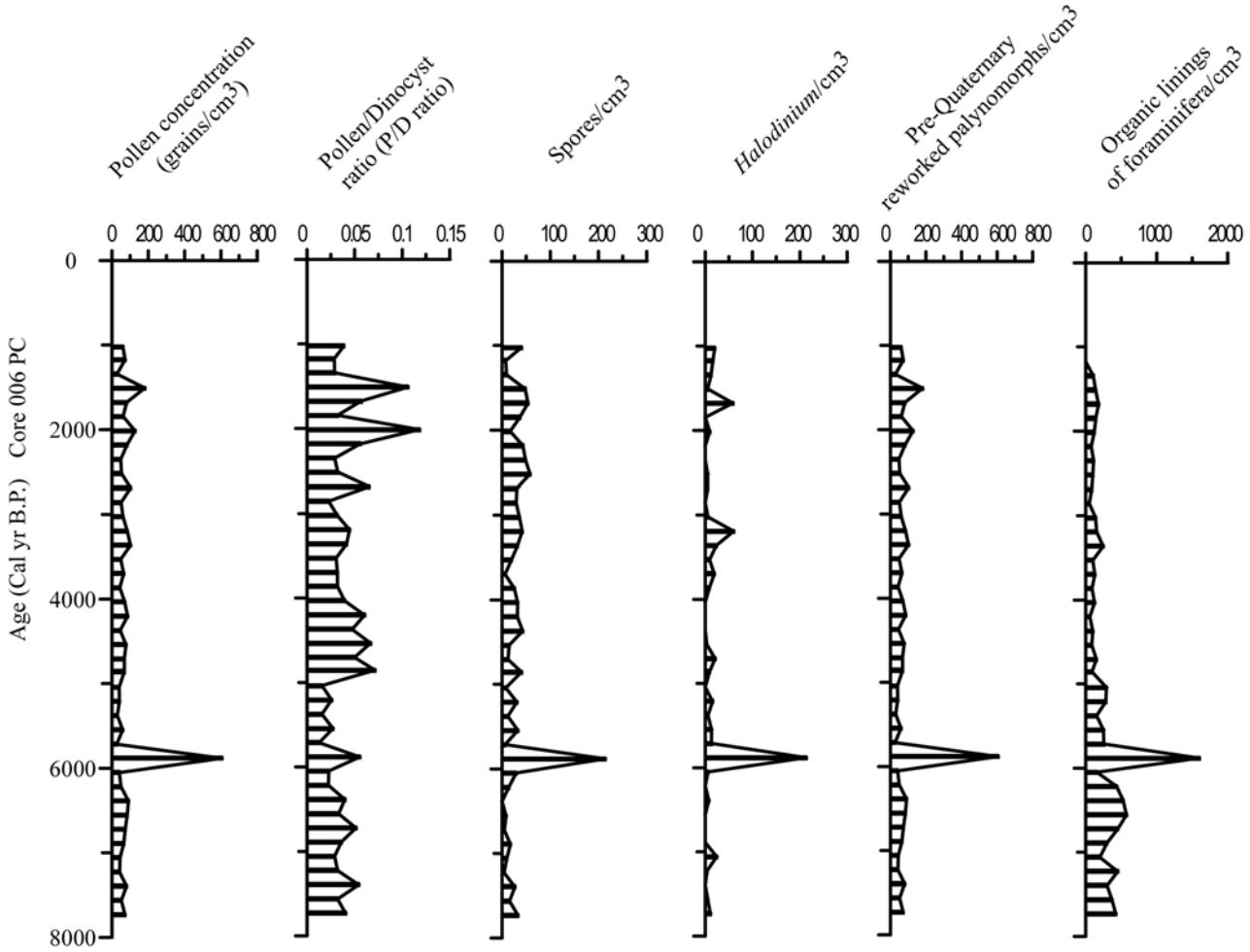

Figure 10. Diagram of pollen, spores, *Halodinium*, pre-Quaternary reworked palynomorphs, and organic linings of foraminifera concentrations. The pollen/dinocyst ratio (P/D ratio) is also shown.

the gradual strengthening of the Irminger and West Greenland Currents as well as the onset of intermediate Labrador Seawater formation [*Hillaire-Marcel et al.*, 2001; *Justwan et al.*, 2008; *Ren et al.*, 2009].

5.2. Middle Holocene in the MANWP: Major Oceanographic and Atmospheric Changes

[25] Dinocyst assemblages, other palynomorph concentrations, quantitative estimates of past sea surface and stable isotopes suggest that the middle Holocene corresponds to a time of important changes in Dease Strait (Figures 9, 10 and 11). Maximum SSTs (~6°C, 2°C warmer than modern conditions) are reached around 5500 cal years B.P., in the lowermost zone II and are 4.5°C greater than those of the uppermost zone I. During the same interval, the reconstructed SSSs (August) also indicate a strong amplitude between the uppermost zone I (value of ~32) and the lowermost zone II (value of ~20). These are also marked by the first occurrence of the heterotrophic taxon *Selenopemphix quanta*. Most important is the abrupt and strong increase of the dinocyst concentrations (from 1800 to 10900 cysts/cm^3) as well as pollen, spores and pre-Quaternary reworked palynomorph concentrations between 6000 and 5500 cal years B.P. (Figures 8, 9 and 10). The relatively high pollen and spore concentrations during this time interval (605 and 213 individuals/cm^3) indicate important continental inputs. The increased concentration of the brackish water algae, *Halodinium* (from ~5 to 213 indivuduals/cm^3), suggests that hydrodynamic transport through river runoff was the main source of the terrestrial palynomorphs. The concentration of organic linings of foraminifers also records a strong increase, which suggests relatively important benthic productivity. This indicates an efficient transfer of organic matter from the surface to the seafloor, probably in a low energy environment. The pollen dinocyst ratio (P/D ratio) also indicates that sea surface production was important despite both a marked increase of the C/N ratio and a strong decrease of the $\delta^{13}C_{org}$, which suggest dominant continental contribution to the organic matter content. The $CaCO_3$ content also depicts a decrease, consistent with low values of the C_{inorg}. Stable isotope records in core from the eastern Chukchi Sea indicate a decrease of the terrestrial organic matter, which began in the middle Holocene and related to a possible more eastward component of the Mackenzie dis-

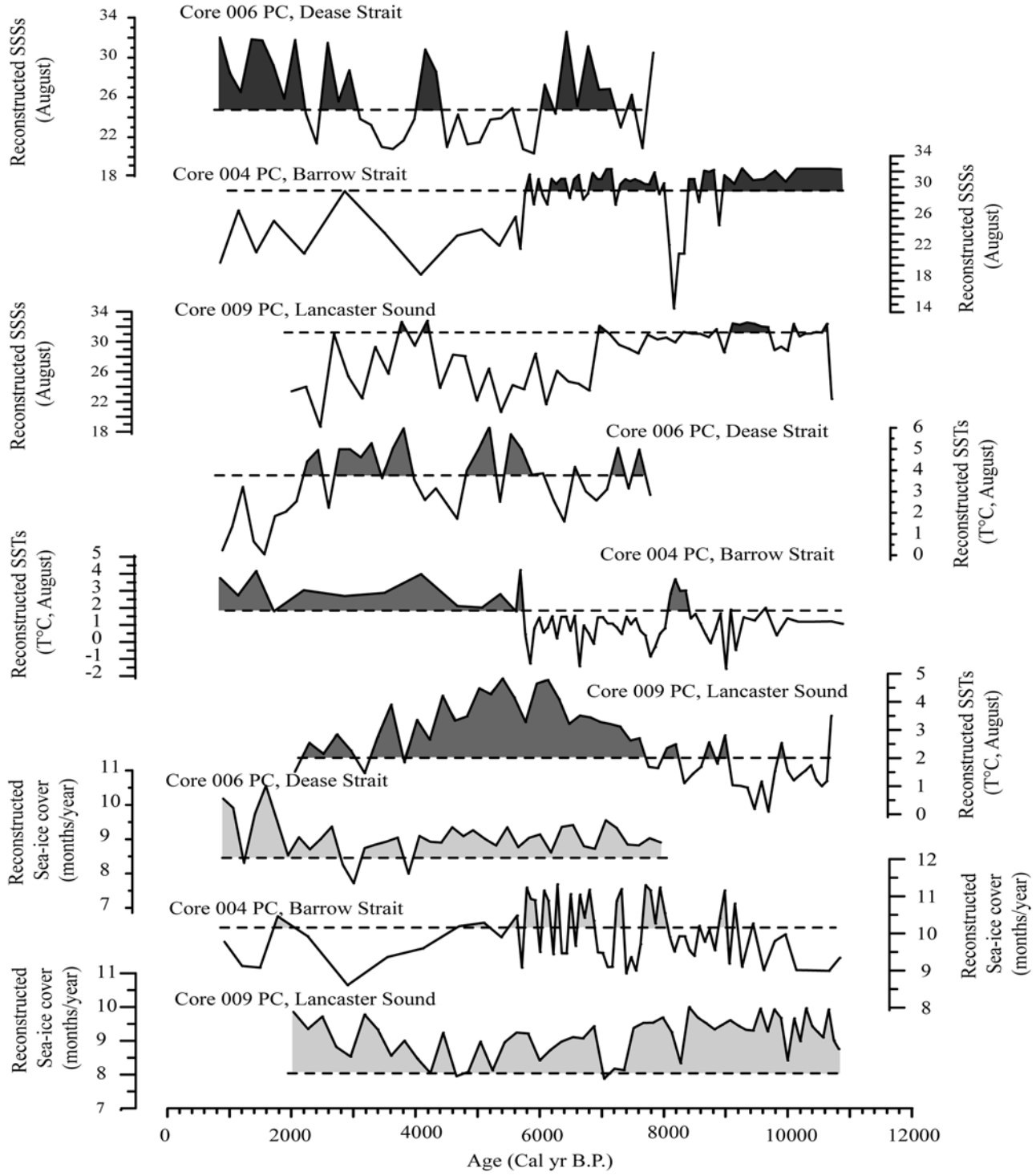

Figure 11. Reconstructed sea surface parameters for cores 009 PC (Lancaster Sound), 004 PC (Barrow Strait), and 006 PC (Dease Strait). The dashed lines correspond to the modern sea surface conditions for each site. The light gray zones are the reconstructed sea ice cover with values higher than modern conditions. The medium gray zones are the reconstructed SSTs (August) with values warmer than modern conditions. The dark gray zones are the reconstructed SSSs (August) with values higher than modern conditions (see text for details).

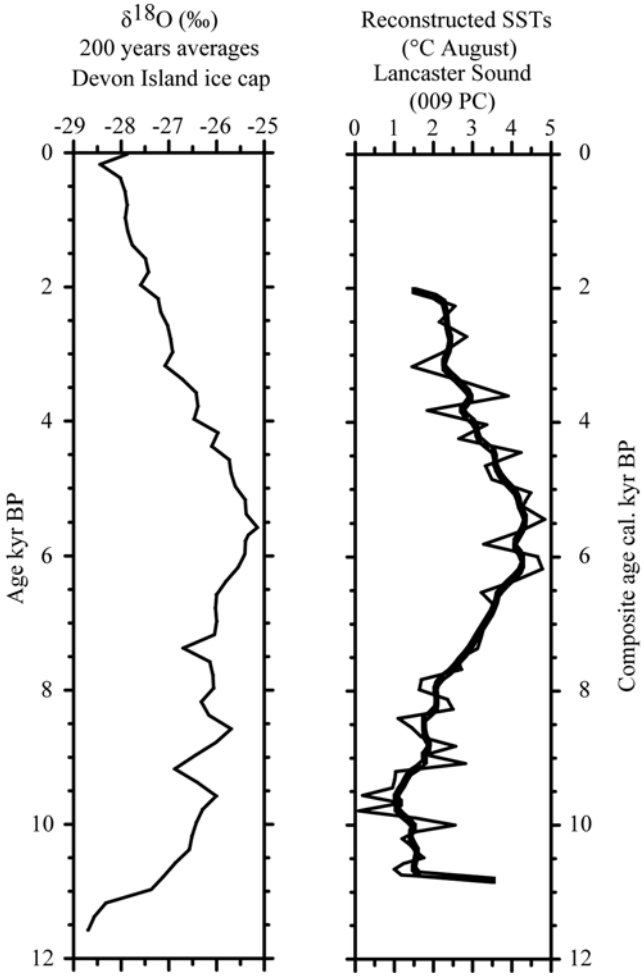

Figure 12. Holocene ice core $\delta^{18}O$ records from Devon Island ice cap (200 years average) versus quantitative estimates of SSTs (August) from Lancaster Sound (core 009 PC). The gray line corresponds to a smoothing curve (10 points) of the reconstructed SST. The comparison of the two diagrams shows the same trend, suggesting a strong oceanic/atmospheric coupling throughout the Holocene in this area (modified from Ledu et al. (submitted manuscript)).

charge [*McKay et al.*, 2008]. Based on driftwood records, *Dyke and Savelle* [2000] found no wood in the western CAA (northwestern Victoria Island) before 4700 cal years B.P. Strong Eurasian rivers discharge during the early to middle Holocene could have abnormally pushed the TPD toward North America. This in turn could have pushed the BG against the Beaufort Sea inner shelf, deflecting the Mackenzie Current toward the west. These are consistent with a possible strong positive mode of the AO during the early Holocene. Based on the mineralogy of silt-sand grains from western Arctic cores, *Darby and Bischof* [2004] have suggested a sea ice drift pattern analogous to the impact of the impact of the AO during this interval. Similarly, based on dinocyst assemblages and pollen records from the Chukchi Sea, the Northwest Passage, the eastern Baffin Island and southwestern Greenland, *de Vernal et al.* [2005a], *McKay et al.* [2008], *Ledu et al.* [2008a, also submitted manuscript] and *Fréchette and de Vernal* [2009] indicate strong cyclonic conditions during the early Holocene. Alkenone and multiproxy records in cores from the Mediterranean Sea, the western subtropical Atlantic, the northern Red Sea and the southwestern Black Sea also suggest climatic conditions similar to the AO during the Holocene [*Rimbu et al.*, 2003; *Lamy et al.*, 2006]. Therefore, strong positive mode of the AO could have operated until the middle Holocene, where more anticyclonic conditions may have reduced the influence of TPD toward North America, allowing the eastward implementation of the Mackenzie Current. Thus, our record in Dease Strait is most likely due to an increase influence of the Mackenzie Current into the western CAA probably due to the implementation of the modern Mackenzie Current as suggested by the lower reconstructed SSSs. This major oceanographic change in the westernmost part of the MANWP is synchronous with important changes in the central and easternmost part of the MANWP (Barrow Strait and Lancaster Sound). Quantitative estimates of SSTs and SSSs (August) in core 004 PC (Barrow Strait) also indicate large amplitude change of temperatures (5°C) and salinity (from 32 to 22) between ~6500 and 6000 cal years B.P., followed by a gradual trend toward warmer conditions (Figure 11). Paleoceanographic records from core 009 PC (Lancaster Sound) suggest a trend toward cooler conditions beginning around 5000 cal years B.P. (Figure 11), which is also recorded by the $\delta^{18}O$ data [*Fisher and Koerner*, 1980] from the Devon Island ice cap (Figure 12). We associate our records in the MANWP in the middle Holocene to major changes in the atmospheric circulation following the early Holocene large-scale oceanic reorganization, which could correspond to a shift toward more anticyclonic conditions (i.e., from AO^+ to AO^-).

5.3. Middle to Late Holocene and a Possible Impact of the Negative Mode of the AO

[26] Quantitative estimates of past sea surface conditions in Dease Strait indicate a cooling trend beginning around 4000 cal years B.P. (Figures 9 and 11). The reconstructed SSTs (August) record minimum values of 0°C (around 2000 cal years B.P.), which is ~4°C lower than modern conditions. These are accompanied by a general increase of both the SSSs (August, maximum of 32) and the sea ice cover (maximum of 10.5 months/year, which is 2 months/year more than modern conditions). This cooling trend corresponds to the uppermost zone II and zone I, where a gradual increase in the relative abundance of *Brigantedinium* spp. and a decrease of the cyst of *Polykrikos* arctic morphotype is observed. These are also accompanied by the complete disappearance of *Selenopemphix quanta* and the gradual decrease of *Operculodinium centrocarpum* and *Spiniferites elongatus/frigidus* in the uppermost zone I. This cooling trend during the late Holocene in Dease Strait contradicts results from other marine records from the western Arctic. Quantitative estimates of past sea surface conditions based on dinocyst assemblages in cores from the Beaufort Sea [*Rochon et al.*, 2006], the eastern and western Chukchi Sea [*McKay et al.*, 2008; *de Vernal et al.*, 2005a] indicate a general trend toward increasing both SSTs and SSSs as well

as decreasing sea ice cover. Similarly, records from core 004 PC (Barrow Strait; Figure 11) suggest warmer conditions with an increase of the reconstructed SSTs (August) accompanied by both a decrease SSSs (August) and sea ice cover [*Ledu et al.*, 2008a, also submitted manuscript]. Under modern conditions, the negative mode of the AO implies less precipitation over the Siberian watershed as well as more advection of Pacific water in the Arctic Ocean [*McLaughlin et al.*, 2004; *Proshutinsky et al.*, 2002; *Häkkinen and Proshutinsky*, 2004; *Steele et al.*, 2004; *Steele and Ermold*, 2004]. In the western Canadian Arctic, the strong northeasterlies reinforced the anticyclonic Beaufort Gyre and enhance upwelling of deep water along the shelf. Taken together, these processes create both a salinification in the western Arctic and positive SST anomalies. Several studies based on pollen, radiocarbon dated fossils, diatoms, aquatic palynomorphs and foraminifers have documented a decrease of freshwater content in the Russian Arctic seas during the middle to late Holocene [*Polyak et al.*, 2002; *Bauch and Polyakova*, 2003; *Prange and Lohmann*, 2003; *Polyakova et al.*, 2005]. These have been associated with a decrease in precipitation over northern Eurasia [*Andreev and Klimanov*, 2000; *MacDonald et al.*, 2000]. During the negative mode of the AO, storm tracks tend to be over the central Arctic rather than over northern Eurasia [*Dickson et al.*, 2000; *Serreze and Barrett*, 2008] consistent with both increase Canadian river and decrease Eurasian river discharge [*Peterson et al.*, 2002; *Déry and Wood*, 2005; *McClelland et al.*, 2006].

[27] Therefore, the trend toward increasing SSSs recorded in cores from the Chukchi Sea [*de Vernal et al.*, 2005a; *McKay et al.*, 2008] between the middle to late Holocene is probably due to a decrease of Russian river discharge together with an increase inflow of Pacific water, which triggered a relative salinification of the surface layer in this area. The sea surface conditions recorded in core 006 PC (Dease Strait) with both the low SSTs (August) and increase reconstructed SSSs (August) is most likely due to vertical mixing between the ACCW (upper summer Pacific halocline) and the wBSW (winter Pacific halocline), which constitute the halocline in this area [*Jones et al.*, 2003; *Steele et al.*, 2004]. The mix of the ACCW with the relatively cold saline nutrient-rich wBSW could have promoted a high abundance of diatoms, which can grow under variable light conditions in cold water [*Agustí and Duarte*, 2000; *Lovejoy et al.*, 2002]. This could explain the gradual decrease in the relative abundance of the phototrophic dinoflagellate and the gradual increase in the relative abundance of the opportunistic heterotrophic taxon *Brigantedinium* spp.

[28] The decreased SSSs (August) and sea ice cover in core 004 PC (Barrow Strait) could be due to the storms track during the negative mode of the AO. In modern conditions, prominent reduction of sea ice concentration in the central Arctic has been linked with well developed cyclone pattern [*Serreze et al.*, 2003; *Serreze and Barrett*, 2008]. Increase in Arctic cyclone activity from 7000 years B.P. has been inferred from pollen records [*Fréchette and de Vernal*, 2009]. The impact of the negative mode of the AO during the middle to late Holocene, is further supported by records from the eastern Arctic. Data from core 009 PC (Lancaster Sound; Figure 11) and northernmost Baffin Bay [*Levac et al.*, 2001; *Rochon et al.*, 2006; *Ledu et al.*, 2008a, also submitted manuscript] indicate higher SSTs than modern conditions but with a cooling trend. Therefore, we associate our record in the MANWP during the middle to late Holocene to the negative mode of the AO operating at the millennial time scale.

5.4. A New Holocene Sea Ice History for the MANWP: A Synthesis Between Qualitative and Quantitative Dinocyst Approaches

[29] Reconstruction of Holocene sea ice history in the MANWP has been mostly inferred from both raised beach bowhead whale and walrus bone remains and driftwood incursions [*Dyke et al.*, 1996, 1997, 2005; *Dyke and Savelle*, 2000, 2001; *Savelle et al.*, 2000; *Dyke and England*, 2003]. Recently, *Vare et al.* [2009] have also proposed a qualitative reconstruction of Holocene sea ice history for the central part of the CAA (Barrow Strait) based on the biomarker IP_{25}. Overall, our records based on dinocyst assemblages are in good agreement with sea ice history in the CAA inferred from bowhead whale remains (Table 3). However, our dinocyst based sea surface reconstructions show several important new features concerning the Holocene sea ice history in the MANWP. The presence of dinocyst throughout the Holocene in cores from Lancaster Sound, Barrow and Dease Straits suggests that the MANWP has already been ice free during the summer over the last 10,000 years. We also found an extensive sea ice cover in the eastern part of the MANWP (Lancaster Sound) for most of the Holocene (Figure 11), whereas bowhead whale remains indicate less sea ice cover from 10,500 to 8500 cal years B.P. and from 5000 to 3000 cal years B.P. [*Dyke et al.*, 1996, 2005]. Our sampling site in Lancaster Sound is located at the southeasternmost part of Devon Island. The comparison between the $\delta^{18}O$ in ice core from Devon ice cap and the reconstructed SSTs (August) from core 009 PC suggests a strong oceanic and atmospheric coupling throughout the Holocene (Figure 12). Although, our record indicates a gradual cooling (SSTs) from the middle to late Holocene, we found that SSTs were warmer than modern conditions over most of the Holocene. We associate the discrepancy between bowhead whale remains and dinocyst sea ice based reconstructions in the easternmost part of the MANWP to the gradual input of local freshwater from the eastern part of the Devon Island ice cap as suggested by the low reconstructed SSSs (August). This local low surface water salinity has probably promoted the formation of a local extensive sea ice cover for most of the Holocene. In modern conditions, the western part of the Devon Island ice cap terminates entirely on land but the eastern part is connected to the sea [*Burgess et al.*, 2005; *Burgess and Sharp*, 2008]. The southeasternmost part of the ice cap is known to be one of the most sensitive to air temperature [*Burgess and Sharp*, 2008; *Colgan et al.*, 2008]. Extensive sea ice cover in the early Holocene is also probably due to the presence of active ice streams in the northernmost Baffin Bay until 8500 cal years B.P. [*England et al.*, 2006; *Dyke*, 2008; Ledu et al., submitted manuscript].

Table 3. Comparison Between Holocene Sea Ice Bowhead Remains Based Reconstructions and Holocene Dinocyst Sea Surface Based Reconstructions in the CAA

MANWP Zone	Bowhead Remains Based Reconstruction Sea Ice Cover Versus Modern Conditions	Dinocyst Based Reconstructions[a]		
		Sea Ice Cover Versus Modern Conditions (months/year)	SSTs Versus Modern Conditions (T°C)	SSSs Versus Modern Conditions
		Modern Conditions		
Eastern		8.1	2	31.3
Central		10.2	1.9	30
Western		8.5	3.9	25
		Historical Changes (~ Last 500 Years)		
Eastern	More	Higher 9.0 (7.8–9.9)[b]	Slightly lower 1.9 (1.2/2.3)	Lower 27.3 (19.5–31.9)
Central	More	Lower 9.7 (9.3–9.9)	Higher 2.9 (1.9/4.1)[b]	Lower 21.9 (20.6/24.8)
Western	More	Higher 10.0 (7.1–11.2)	Lower 0.7 (−0.3/5.1)	Higher 31.3 (27.5/33.1)
		Middle-Late Holocene (After ca 6,000)		
Eastern	Less	Higher 8.9 (7.9–9.8)	Higher 3.1 (1.4/4.8)[b]	Lower 25.9 (18.6–32.7)
Central	Less	Lower 9.9 (8.6–11.2)	Higher 2.3 (−1.2/4.0)	Lower 24.7 (18.8/31.6)
Western	More	Higher 9.0 (7.7–10.5)	Lower 3.4 (0.0/6.0)	Slightly higher 25.4 (20.3/32)
		Early Middle Holocene (ca 8,500 to 6,000)		
Eastern	More	Higher 8.9 (7.8–10.0)	Higher 2.9 (1.1/4.7)	Lower 28.2 (21.6–32.1)
Central	More	Slightly lower 10.1 (8.9–11.3)[c]	Lower 1.0 (−1.4/3.6)	Lower 29.2 (14.4/32.3)
Western	More	Slightly higher 9.0 (8.6–9.5)	Lower 3.3 (1.5/5.0)	Slightly higher 26.2 (20.3/32.5)
		Early Holocene (ca 10,800 to 8,500)		
Eastern	Less	Higher 9.4 (8.4–9.9)	Lower 1.5 (0.0/3.5)	Lower 30.7 (22.3/32.5)
Central	Less	Lower 9.6 (8.9–11.1)	Lower 0.9 (−1.5/2.0)	Higher 31.1 (25.1/32.4)
Western	Less	No records	No records	No records

[a]The first number is the average for each time interval, and the numbers in parentheses are the minimum and maximum values derived from the modern analog technique (MAT). Note that the dinocyst quantitative reconstructions are based on the best estimates, which are the averages of hydrographic parameters weighted inversely to the distance for the five best modern analogs.
[b]With a general cooling trend (see text for details).
[c]With large fluctuations.

[30] The bowhead whale remains and dinocyst-based Holocene sea ice reconstructions in the MANNWP may indicate the following conditions.

[31] 1. There is less sea ice cover than modern conditions in most of the MANWP during the early Holocene (from 10,800 to ~8500 cal years B.P.) but with more sea ice in few areas (e.g., Lancaster Sound), which indicate a more pronounced regionalism than previously reported by the bowhead whale remains records (see *Dyke et al.* [2005] for a synthesis on the subject).

[32] 2. There is more sea ice cover than modern conditions in the easternmost part of the MANWP but with millennial-scale sea ice fluctuations in the central part of the MANWP during the early middle Holocene (from ~8500 to ~6000 cal years B.P.). The westernmost part of the MANWP indicates little changes with respect to modern conditions.

[33] 3. There is more sea ice cover than modern conditions in the easternmost part of the MANWP from the middle to late Holocene (after ~6000 cal years B.P.). In contrast, a decrease of the sea ice cover is recorded in the central part of the MANWP with respect to modern conditions. The record in the westernmost part of the MANWP suggests little changes from 6000 to 4000 cal years B.P. A slight increase of the sea ice cover is indicated after 4000 cal years B.P.

6. Summary and Conclusion

[34] Cores 006, 004 and 009 provide the first quantitative records of sea surface conditions in the MANWP for most of the Holocene. The early Holocene (from ~11000 to ~8500 cal years B.P.) is characterized by strong terrigenous inputs in the easternmost and central part of the MANWP associated with the last phase of the Innuitian deglaciation (for details see *Ledu et al.* [2008a, 2008b, also submitted manuscript]). During this interval, several active ice streams, in the northernmost Baffin Bay, promoted an extensive sea ice cover in Lancaster Sound. Maximum ice thickness in the central north CAA together with the presence of the Wellington channel ice stream have probably created more unstable conditions in Barrow Strait (Ledu et al., submitted manuscript). The early middle Holocene (from ~8000 to ~6000 cal years B.P.) was marked by opposite trend between the western central and eastern part of the MANWP. Maximum influence of the warm intermediate Atlantic water together with increase air temperatures [*de Vernal and Hillaire-Marcel*, 2006] have probably enhanced terrestrial ice melt on Devon Island ice cap and local freshwater input. This led to a relatively extensive sea ice cover in Lancaster Sound. The western central Arctic was marked by a sharp halocline promoting the formation of sea ice [*de Vernal et al.*, 2005a; *McKay et al.*, 2008]. We associate the climate variability in the MANWP during the early middle Holocene to a strong positive mode of the AO operating at the millennial time scale. This is consistent with a strong divergence in the eastern Arctic, which triggered positive SST anomalies and a marked convergence with increased Eurasian river runoff, which enhanced negative SST anomalies and extensive sea ice cover in the western Arctic. This was accom-

panied by major oceanographic changes, including the gradual implementation of the modern West Greenland and Irminger Currents as well as the development of an active site of intermediate Labrador Seawater formation [*Hillaire-Marcel et al.*, 2001; *Justwan et al.*, 2008; *Ren et al.*, 2009]. The middle Holocene (around 6000 cal years B.P.) in the westernmost and central part of the MANWP (Dease and Barrow Strait) is marked by a thermal amplitude as much as ~5°C. Records from the easternmost part of the MANWP (Lancaster Sound) indicate the onset of a trend toward cooler conditions. In Dease Strait, this was probably accompanied by the implementation of the modern Mackenzie Current in a low energy environment. We associate the climate variability in the MANWP during the middle Holocene to a change in atmospheric circulation related to a shift of the AO (from AO^+ to AO^-). The middle to late Holocene (after ~6000 cal years B.P.) is characterized by harsh conditions in the westernmost part of the MANWP, whereas records from the Chukchi Sea [*de Vernal et al.*, 2005a; *McKay et al.*, 2008] and the central part of the MANWP (Barrow Strait) [*Ledu et al.*, 2008b, also submitted manuscript] indicate warmer conditions. We associate these conditions in Dease Strait with vertical mixing between the summer and cold nutrient-rich winter Pacific water. Records from the easternmost part of the MANWP (Lancaster Sound) indicate a gradual cooling, which highlighted the dipolar structure between the eastern and western Arctic similar to the impact of the AO. Therefore, climate variability in the MANWP during the middle-late Holocene is associated with the dominance of negative AO mode accompanied by northeasterly winds inducing upwelling along the western coast of the CAA.

[35] At the scale of the Holocene, our records suggest that the climate variability in the MANWP is strongly influenced by large-scale atmospheric patterns, such as the AO, operating at the millennial time scale. However, local conditions may create a marked regionalism highlighting the strong heterogeneity of the Arctic Ocean.

[36] **Acknowledgments.** This work was funded by the ArcticNet Network of Centres of Excellence and the Natural Science and Engineering Research Council of Canada (NSERC). This is a contribution to the ArcticNet project 1.6 (The Opening NW Passage: Resources, Navigation, Sovereignty & Security), the Polar Climate Stability Network supported by the Canadian Foundation for Climate and Atmospheric Science, and the NSERC-IPY project "Natural climate variability and forcings in Canadian Arctic and Arctic Ocean." We wish to thank the officers and crew of the CCGS *Amundsen* for their help and support during sampling. We also wish to express our gratitude to the following people who helped during the collection and analysis of the samples: Robbie Bennett, Bedford Institute of Oceanography; Trecia Schell, Dalhousie University; Sylvain Leblanc, Pierre Simard, and Guillaume Auclair, UQAR. Thanks are due to Bassam Ghaleb and Jean-François Hélie (GEOTOP) for geochemical and isotope analyses. We also wish to thank Monika Korte for the CALS7K.2 inclination data at the sites of cores 006, 004, and 009 PC. Finally, we are grateful to the two anonymous reviewers for their comments, which helped to improve the manuscript.

References

Agustí, S., and C. M. Duarte (2000), Experimental induction of a large phytoplankton bloom in Antarctic coastal waters, *Mar. Ecol. Prog. Ser.*, *206*, 73–85, doi:10.3354/meps206073.

Andreev, A. A., and V. A. Klimanov (2000), Quantitative Holocene climatic reconstruction from Arctic Russia, *J. Paleolimnol.*, *24*, 81–91, doi:10.1023/A:1008121917521.

Andrews, J. T., and A. E. Jennings (1990), Geomagnetic secular variations (inclination) of high latitude fjord cores: Eastern Canadian Arctic, *Polar Res.*, *8*, 245–259, doi:10.1111/j.1751-8369.1990.tb00387.x.

Barletta, F., G. St-Onge, J. E. T. Channell, A. Rochon, L. Polyak, and D. Darby (2008a), High-resolution paleomagnetic secular variation and relative paleointensity records from the western Canadian Arctic: Implication for Holocene stratigraphy and geomagnetic field behaviour, *Can. J. Earth Sci.*, *45*, 1265–1281, doi:10.1139/E08-039.

Barletta, F., G. St-Onge, and A. Rochon (2008b), Paleomagnetic dating of Holocene western Canadian Arctic sediments: Combined use of secular variation and time-varying spherical harmonic model of the geomagnetic field, paper presented at Arctic Change 2008, Int. Polar Year, Quebec City, Que., Canada.

Bauch, H. A., and Y. I. Polyakova (2003), Diatom-inferred salinity records from the Arctic Siberian margin: Implications for fluvial runoff patterns during the Holocene, *Paleoceanography*, *18*(2), 1027, doi:10.1029/2002PA000847.

Besonen, M. R., W. Patridge, R. S. Bradley, P. Francus, J. S. Stoner, and M. B. Abbott (2008), A record of climate over the last millennium based on varved lake sediments from the Canadian High Arctic, *Holocene*, *18*, 169–180, doi:10.1177/0959683607085607.

Blott, S. J., and K. Pye (2001), GRADISTAT: A grain size distribution and statistics package for the analysis of unconsolidated sediments, *Earth Surf. Processes Landforms*, *26*, 1237–1248, doi:10.1002/esp.261.

Breckenridge, A., T. C. Johnson, S. Beske-Diehl, and J. S. Mothersill (2004), The timing of regional lateglacial events and post-glacial sedimentation rates from Lake Superior, *Quat. Sci. Rev.*, *23*, 2355–2367, doi:10.1016/j.quascirev.2004.04.007.

Burgess, D., and M. J. Sharp (2008), Recent changes in thickness of the Devon Island ice cap, Canada, *J. Geophys. Res.*, *113*, B07204, doi:10.1029/2007JB005238.

Burgess, D. O., M. J. Sharp, D. W. F. Mair, J. A. Dowdeswell, and T. J. Benham (2005), Flow dynamics and iceberg calving rates of Devon Ice Cap, Nunavut, Canada, *J. Glaciol.*, *51*, 219–230, doi:10.3189/172756505781829430.

Butler, R. F. (1992), *Paleomagnetism: Magnetic Domains to Geologic Terranes*, 319 pp., Blackwell, Oxford, U. K.

Carmack, E., F. McLaughlin, M. Yamamoto-Kawai, M. Itoh, K. Shimada, R. Krishfield, and A. Proshutinsky (2008), Freshwater storage in the Northern Ocean and the special role of the Beaufort Gyre, in *Arctic-Subarctic Ocean Fluxes: Defining the Role of the Northern Seas in Climate*, edited by R. R. Dickson, J. Meincke, and P. Rhines, pp. 145–170, Springer, Dordrecht, Netherlands.

Colgan, W., J. Davis, and M. Sharp (2008), Is the high-elevation region of Devon Ice Cap thickening?, *J. Glaciol.*, *54*, 428–436, doi:10.3189/002214308785837084.

Comiso, J. C., C. L. Parkinson, R. Gersten, and L. Stock (2008), Accelerated decline in the Arctic sea ice cover, *Geophys. Res. Lett.*, *35*, L01703, doi:10.1029/2007GL031972.

Darby, D. A., and J. F. Bischof (2004), A Holocene record of changing Arctic Ocean ice drift analogous to the effects of the Arctic Oscillation, *Paleoceanography*, *19*, PA1027, doi:10.1029/2003PA000961.

Déry, S. J., and E. F. Wood (2005), Decreasing river discharge in northern Canada, *Geophys. Res. Lett.*, *32*, L10401, doi:10.1029/2005GL022845.

Deser, C., and H. Teng (2008), Evolution of Arctic sea ice concentration trends and the role of atmospheric circulation forcing, 1979–2007, *Geophys. Res. Lett.*, *35*, L02504, doi:10.1029/2007GL032023.

de Vernal, A., and C. Hillaire-Marcel (2006), Provincialism in trends and high frequency changes in the northwest North Atlantic during the Holocene, *Global Planet. Change*, *54*, 263–290, doi:10.1016/j.gloplacha.2006.06.023.

de Vernal, A., and F. Marret (2007), Organic-walled dinoflagellate cysts: Tracers of sea-surface conditions, in *Proxies in Late Cenozoic Paleoceanography*, edited by C. Hillaire-Marcel and A. de Vernal, pp. 371–408, doi:10.1016/S1572-5480(07)01014-7, Elsevier, Amsterdam.

de Vernal, A., et al. (2001), Dinoflagellate cyst assemblages as tracers of sea-surface conditions in the northern North Atlantic, Arctic and sub-Arctic seas: The new '$n = 677$' data base and its application for quantitative palaeoceanographic reconstruction, *J. Quat. Sci.*, *16*, 681–698, doi:10.1002/jqs.659.

de Vernal, A., C. Hillaire-Marcel, and D. A. Darby (2005a), Variability of sea ice cover in the Chukchi Sea (western Arctic Ocean) during the

Holocene, *Paleoceanography*, *20*, PA4018, doi:10.1029/2005PA001157.

de Vernal, A., et al. (2005b), Reconstruction of sea-surface conditions at middle to high latitudes of the Northern Hemisphere during the Last Glacial Maximum (LGM) based on dinoflagellate cyst assemblages, *Quat. Sci. Rev.*, *24*, 897–924, doi:10.1016/j.quascirev.2004.06.014.

Dickson, R. R., T. J. Osborn, J. W. Hurrell, J. Meincke, J. Blindheim, B. Adlandsvik, T. Vinje, G. Alekseev, and W. Maslowski (2000), The Arctic Ocean response to the North Atlantic Oscillation, *J. Clim.*, *13*, 2671–2696, doi:10.1175/1520-0442(2000)013<2671:TAORTT>2.0.CO;2.

Dukhovskoy, D. S., M. A. Johnson, and A. Proshutinsky (2004), Arctic decadal variability: An auto-oscillatory system of heat and fresh water exchange, *Geophys. Res. Lett.*, *31*, L03302, doi:10.1029/2003GL019023.

Dunlop, D. J., and Ö. Özdemir (1997), *Rock Magnetism: Fundamentals and Frontiers*, *Cambridge Stud. Magn. Ser.*, vol. 3, 573 pp., Cambridge Univ. Press, Cambridge, U. K.

Duplessy, J. C., E. Cortijo, E. Ivanova, T. Khusid, L. Labeyrie, M. Levitan, I. Murdmaa, and M. Paterne (2005), Paleoceanography of the Barents Sea during the Holocene, *Paleoceanography*, *20*, PA4004, doi:10.1029/2004PA001116.

Dyke, A. S. (2008), The Steensby Inlet Ice Stream in the context of the deglaciation of northern Baffin Island, eastern Arctic Canada, *Earth Surf. Processes Landforms*, *33*, 573–592, doi:10.1002/esp.1664.

Dyke, A. S., and J. England (2003), Canada's most northerly postglacial bowhead whales (*Balaena mysticetus*): Holocene sea-ice conditions and polynya development, *Arctic*, *56*, 14–20.

Dyke, A. S., and J. M. Savelle (2000), Holocene driftwood incursion to southwestern Victoria Island, Canadian Arctic Archipelago, and its significance to paleoceanography and archaeology, *Quat. Res.*, *54*, 113–120, doi:10.1006/qres.2000.2141.

Dyke, A. S., and J. M. Savelle (2001), Holocene history of the Bering Sea bowhead whale (*Balaena mysticetus*) in its Beaufort Sea summer grounds off southwestern Victoria Island, western Canadian Arctic, *Quat. Res.*, *55*, 371–379, doi:10.1006/qres.2001.2228.

Dyke, A. S., J. Hooper, and J. M. Savelle (1996), A history of sea ice in the Canadian Arctic Archipelago based on postglacial remains of the bowhead whale (*Balaena mysticetus*), *Arctic*, *49*, 235–255.

Dyke, A. S., J. England, E. Reimnitz, and H. Jette (1997), Changes in driftwood delivery to the Canadian arctic archipelago: The hypothesis of postglacial oscillations of the transpolar drift, *Arctic*, *50*, 1–16.

Dyke, A. S., J. M. Savelle, and D. A. Hodgson (2005), Environmental history and archaeology along the Northwest Passage: Water, ice, and life—The Quaternary interface, paper presented at Canadian Quaternary Association Conference, Univ. of MB, Winnipeg, MB, Canada.

England, J., N. Atkinson, J. Bednarski, A. S. Dyke, D. A. Hodgson, and C. Ó. Cofaigh (2006), The Innuitian Ice Sheet: Configuration, dynamics and chronology, *Quat. Sci. Rev.*, *25*, 689–703, doi:10.1016/j.quascirev.2005.08.007.

Fisher, D. A., and R. M. Koerner (1980), Some aspects of climatic change in the High Arctic during the Holocene as deduced from ice cores, in *Quaternary Paleoclimate*, edited by W. C. Mahaney, pp. 349–371, GeoAbstracts, Norwich, U. K.

Fréchette, B., and A. de Vernal (2009), Relationship between Holocene climate variations over southern Greenland and eastern Baffin Island and synoptic circulation pattern, *Clim. Past*, *5*, 347–359.

Guiot, J., and A. de Vernal (2007), Transfer functions: Methods for quantitative paleoceanography based on microfossils, in *Proxies in Late Cenozoic Paleoceanography*, edited by C. Hillaire-Marcel and A. de Vernal, pp. 523–563, Elsevier, Amsterdam.

Häkkinen, S., and A. Proshutinsky (2004), Freshwater content variability in the Arctic Ocean, *J. Geophys. Res.*, *109*, C03051, doi:10.1029/2003JC001940.

Hamel, D., A. de Vernal, M. Gosselin, and C. Hillaire-Marcel (2002), Organic-walled microfossils and geochemical tracers: Sedimentary indicators of productivity changes in the North Water and northern Baffin Bay during the last centuries, *Deep Sea Res., Part II*, *49*, 5277–5295.

Head, M. J., R. Harland, and J. Matthiessen (2001), Cold marine indicators of the late Quaternary: The new dinoflagellate cyst genus *Islandinium* and related morphotypes, *J. Quat. Sci.*, *16*, 621–636, doi:10.1002/jqs.657.

Hillaire-Marcel, C., A. de Vernal, G. Bilodeau, and A. J. Weaver (2001), Absence of deep-water formation in the Labrador Sea during the last interglacial period, *Nature*, *410*, 1073–1077, doi:10.1038/35074059.

Hillaire-Marcel, C., A. de Vernal, L. Polyak, and D. Darby (2004), Size-dependent isotopic composition of planktic foraminifers from Chukchi Sea vs. NW Atlantic sediments—Implications for the Holocene paleoceanography of the western Arctic, *Quat. Sci. Rev.*, *23*, 245–260, doi:10.1016/j.quascirev.2003.08.006.

Jakobsson, M. (2002), Hypsometry and volume of the Arctic Ocean and its constituent seas, *Geochem. Geophys. Geosyst.*, *3*(5), 1028, doi:10.1029/2001GC000302. (Correction, *Geochem. Geophys. Geosyst.*, *5*, Q02005, doi:10.1029/2004GC000694, 2004.)

Jones, E. P., J. H. Swift, L. G. Anderson, M. Lipizer, G. Civitarese, K. K. Falkner, G. Kattner, and F. McLaughlin (2003), Tracing Pacific water in the North Atlantic Ocean, *J. Geophys. Res.*, *108*(C4), 3116, doi:10.1029/2001JC001141.

Justwan, A., N. Koc, and A. E. Jennings (2008), Evolution of the Irminger and East Icelandic Current systems through the Holocene, revealed by diatom-based sea surface temperature reconstructions, *Quat. Sci. Rev.*, *27*, 1571–1582, doi:10.1016/j.quascirev.2008.05.006.

Kirschvink, J. L. (1980), The least-squares line and plane and the analysis of paleomagnetic data, *Geophys. J. R. Astron. Soc.*, *62*, 699–718.

Kokinos, J. P., T. I. Eglinton, M. A. Goni, J. J. Boon, P. A. Martoglio, and D. M. Anderson (1998), Characterization of a highly resistant biomacromolecular material in the cell wall of a marine dinoflagellate resting cyst, *Org. Geochem.*, *28*, 265–288, doi:10.1016/S0146-6380(97)00134-4.

Korte, M., and C. G. Constable (2005), Continuous geomagnetic field models for the past 7 millennia: 2. CALS7K, *Geochem. Geophys. Geosyst.*, *6*, Q02H16, doi:10.1029/2004GC000801.

Kotilainen, A. T., T. Saarinen, and B. Winterhalter (2000), High-resolution paleomagnetic dating of sediments deposited in the central Baltic Sea during the last 3000 years, *Mar. Geol.*, *166*, 51–64, doi:10.1016/S0025-3227(00)00012-8.

Lamy, F., H. W. Arz, G. C. Bond, A. Bahr, and J. Pätzold (2006), Multicentennial-scale hydrological changes in the Black Sea and northern Red Sea during the Holocene and the Arctic/North Atlantic Oscillation, *Paleoceanography*, *21*, PA1008, doi:10.1029/2005PA001184.

Ledu, D., A. Rochon, A. de Vernal, and G. St-Onge (2008a), Palynological evidence of Holocene climate oscillations in the eastern Arctic: A possible shift in the Arctic Oscillation at the millennial time scale, *Can. J. Earth Sci.*, *45*, 1363–1375, doi:10.1139/E08-043.

Ledu, D., A. Rochon, A. de Vernal, and G. St-Onge (2008b), Holocene climate changes in the main axis of the Northwest Passage inferred from dinocyst assemblages: A possible influence of the Arctic Oscillation at the millennial time scale, paper presented at Arctic Change 2008, Int. Polar Year, Quebec City, Que., Canada.

Levac, E., A. de Vernal, and W. Blake (2001), Sea-surface conditions in northernmost Baffin Bay during the Holocene: Palynological evidence, *J. Quat. Sci.*, *16*, 353–363, doi:10.1002/jqs.614.

Lisé-Pronovost, A., G. St-Onge, S. Brachfeld, F. Barletta, and D. Darby (2009), Paleomagnetic constraints on the Holocene stratigraphy of the Arctic Alaskan margin, *Global Planet. Change*, *68*, 85–99, doi:10.1016/j.gloplacha.2009.03.015.

Lloyd, J. M., L. A. Park, B. Kuijpers, and M. Moros (2005), Early Holocene palaeoceanography and deglacial chronology of Disko Bugt, West Greenland, *Quat. Sci. Rev.*, *24*, 1741–1755, doi:10.1016/j.quascirev.2004.07.024.

Lovejoy, C., L. Legendre, and N. M. Price (2002), Prolonged diatom blooms and microbial food web dynamics: Experimental results from an Arctic polynya, *Aquat. Microb. Ecol.*, *29*, 267–278, doi:10.3354/ame029267.

Lund, S. P. (1996), A comparison of Holocene paleomagnetic secular variation records from North America, *J. Geophys. Res.*, *101*, 8007–8024, doi:10.1029/95JB00039.

MacDonald, G., B. Felzer, B. Finney, and S. Forman (2000), Holocene lake sediment records of Arctic hydrology, *J. Paleolimnol.*, *24*, 1–13, doi:10.1023/A:1008100714795.

McClelland, J. W., S. J. Déry, B. J. Peterson, R. M. Holmes, and E. F. Wood (2006), A pan-arctic evaluation of changes in river discharge during the latter half of the 20th century, *Geophys. Res. Lett.*, *33*, L06715, doi:10.1029/2006GL025753.

McKay, J. L., A. de Vernal, C. Hillaire-Marcel, C. Not, L. Polyak, and D. Darby (2008), Holocene fluctuations in Arctic sea-ice cover: Dinocyst-based reconstructions for the eastern Chukchi Sea, *Can. J. Earth Sci.*, *45*, 1377–1397.

McLaughlin, F. A., E. C. Carmack, R. W. MacDonald, H. Melling, J. H. Swift, P. A. Wheeler, B. F. Sherr, and E. B. Sherr (2004), The joint roles of Pacific and Atlantic-origin waters in the Canada Basin, 1997–1998, *Deep Sea Res., Part I*, *51*, 107–128, doi:10.1016/j.dsr.2003.09.010.

Mudie, P. J., and A. Rochon (2001), Distribution of dinoflagellate cysts in the Canadian Arctic

marine region, *J. Quat. Sci.*, *16*, 603–620, doi:10.1002/jqs.658.

National Oceanography Data Center (NODC) (2001), World Ocean Atlas 2001, http://www.nodc.noaa.gov/OC5/WOA01/pr_woa01.html, Silver Spring, Md.

National Snow and Ice Data Center (NSIDC) (1953–2000), Mean sea-ice extent and concentration, http://nsidc.org/data/seaice/index.html, Boulder, Colo.

Overland, J. E., M. Wang, and S. Salo (2008), The recent Arctic warm period, *Tellus, Ser. A*, *60*, 589–597.

Peterson, B. J., R. M. Holmes, J. W. McClelland, C. J. Vorosmarty, R. B. Lammers, A. I. Shiklomanov, I. A. Shiklomanov, and S. Rahmstorf (2002), Increasing river discharge to the Arctic Ocean, *Science*, *298*, 2171–2173, doi:10.1126/science.1077445.

Polyak, L., M. Levitan, T. Khusid, L. Merklin, and V. Mukhina (2002), Variations in the influence of riverine discharge on the Kara Sea during the last deglaciation and the Holocene, *Global Planet. Change*, *32*, 291–309, doi:10.1016/S0921-8181(02)00072-3.

Polyakov, I. V., and M. A. Johnson (2000), Arctic decadal and interdecadal variability, *Geophys. Res. Lett.*, *27*, 4097–4100, doi:10.1029/2000GL011909.

Polyakov, I. V., G. V. Alekseev, L. A. Timokhov, U. S. Bhatt, R. L. Colony, H. L. Simmons, D. Walsh, J. E. Walsh, and V. F. Zakharov (2004), Variability of the intermediate Atlantic water of the Arctic Ocean over the last 100 years, *J. Clim.*, *17*, 4485–4497, doi:10.1175/JCLI-3224.1.

Polyakova, Y. I., H. A. Bauch, and T. S. Klyuvitkina (2005), Early to middle Holocene changes in Laptev Sea water masses deduced from diatom and aquatic palynomorph assemblages, *Global Planet. Change*, *48*, 208–222, doi:10.1016/j.gloplacha.2004.12.014.

Prange, M., and G. Lohmann (2003), Effects of mid-Holocene river runoff on the Arctic Ocean/sea-ice system: A numerical model study, *Holocene*, *13*, 335–342, doi:10.1191/0959683603hl626rp.

Prinsenberg, S. J., and J. Hamilton (2005), Monitoring the volume, freshwater and heat fluxes passing through Lancaster Sound in the Canadian Arctic Archipelago, *Atmos. Ocean*, *43*, 1–22, doi:10.3137/ao.430101.

Proshutinsky, A., R. H. Bourke, and F. A. McLaughlin (2002), The role of the Beaufort Gyre in Arctic climate variability: Seasonal to decadal climate scales, *Geophys. Res. Lett.*, *29*(23), 2100, doi:10.1029/2002GL015847.

Radi, T., and A. de Vernal (2008), Dinocysts as proxy of primary productivity in mid–high latitudes of the Northern Hemisphere, *Mar. Micropaleontol.*, *68*, 84–114, doi:10.1016/j.marmicro.2008.01.012.

Ren, J., H. Jiang, M. S. Seidenkrantz, and A. Kuijpers (2009), A diatom-based reconstruction of early Holocene hydrographic and climatic change in a southwest Greenland fjord, *Mar. Micropaleontol.*, *70*, 166–176, doi:10.1016/j.marmicro.2008.12.003.

Richerol, T., A. Rochon, S. Blasco, D. B. Scott, T. M. Schell, and R. J. Bennett (2008a), Distribution of dinoflagellate cysts in surface sediments of the Mackenzie Shelf and Amundsen Gulf, Beaufort Sea (Canada), *J. Mar. Syst.*, *74*, 825–839, doi:10.1016/j.jmarsys.2007.11.003.

Richerol, T., A. Rochon, S. Blasco, D. B. Scott, T. M. Schell, and R. J. Bennett (2008b), Evolution of paleo sea-surface conditions over the last 600 years in the Mackenzie Trough, Beaufort Sea (Canada), *Mar. Micropaleontol.*, *68*, 6–20, doi:10.1016/j.marmicro.2008.03.003.

Rigor, I. G., J. M. Wallace, and R. L. Colony (2002), Response of sea ice to the Arctic Oscillation, *J. Clim.*, *15*, 2648–2663, doi:10.1175/1520-0442(2002)015<2648:ROSITT>2.0.CO;2.

Rimbu, N., G. Lohmann, J.-H. Kim, H. W. Arz, and R. Schneider (2003), Arctic/North Atlantic Oscillation signature in Holocene sea surface temperature trends as obtained from alkenone data, *Geophys. Res. Lett.*, *30*(6), 1280, doi:10.1029/2002GL016570.

Rochon, A., A. de Vernal, J.-L. Turon, J. Matthiessen, and M. J. Head (1999), Distribution of recent dinoflagellate cysts in surface sediments from the North Atlantic and adjacent seas, and quantitative reconstruction of sea-surface parameters, *Am. Assoc. Stratigr. Palynol. Contrib. Ser.*, *35*, 150.

Rochon, A., D. B. Scott, T. M. Schell, S. Blasco, R. J. Bennett, and P. J. Mudie (2006), Evolution of sea surface conditions during the Holocene: Comparison between eastern (Baffin Bay and Hudson Strait) and western (Beaufort Sea) Canadian Arctic, *Eos Trans. AGU*, *87*(52), Fall Meet. Suppl., Abstract U43B-0867.

Saarinen, T. (1998), High-resolution palaeosecular variation in northern Europe during the last 3200 years, *Phys. Earth Planet. Inter.*, *106*, 299–309, doi:10.1016/S0031-9201(97)00113-1.

Saarinen, T. (1999), Palaeomagnetic dating of late Holocene sediments in Fennoscandia, *Quat. Sci. Rev.*, *18*, 889–897, doi:10.1016/S0277-3791(99)00003-7.

Savelle, J. M., A. S. Dyke, and A. P. McCartney (2000), Holocene bowhead whale (*Balaena mysticetus*) mortality patterns in the Canadian Arctic Archipelago, *Arctic*, *53*, 414–421.

Schlosser, P., R. Newton, B. Ekwurzel, S. Khatiwala, R. Mortlock, and R. Fairbanks (2002), Decrease of river runoff in the upper waters of the Eurasian Basin, Arctic Ocean, between 1991 and 1996: Evidence from $\delta^{18}O$ data, *Geophys. Res. Lett.*, *29*(9), 1289, doi:10.1029/2001GL013135.

Schweiger, A. J., R. W. Lindsay, S. Vavrus, and J. A. Francis (2008), Relationships between Arctic sea ice and clouds during autumn, *J. Clim.*, *21*, 4799–4810, doi:10.1175/2008JCLI2156.1.

Serreze, M. C., and A. P. Barrett (2008), The summer cyclone maximum over the central Arctic Ocean, *J. Clim.*, *21*, 1048–1065, doi:10.1175/2007JCLI1810.1.

Serreze, M. C., J. A. Maslanik, T. A. Scambos, F. Fetterer, J. Stroeve, K. Knowles, C. Fowler, S. Drobot, R. G. Barry, and T. M. Haran (2003), A new record minimum Arctic sea ice and extent and area in 2002, *Geophys. Res. Lett.*, *30*(3), 1110, doi:10.1029/2002GL016406.

Shimada, K., E. C. Carmack, K. Hatakeyama, and T. Takizawa (2001), Varieties of shallow temperature maximum waters in the Western Canadian Basin of the Arctic Ocean, *Geophys. Res. Lett.*, *28*, 3441–3444, doi:10.1029/2001GL013168.

Ślubowska-Woldengen, M., N. Koç, T. L. Rasmussen, D. Klitgaard-Kristensen, M. Hald, and A. E. Jennings (2008), Time-slice reconstructions of ocean circulation changes on the continental shelf in the Nordic and Barents seas during the last 16,000 cal yr B.P., *Quat. Sci. Rev.*, *27*, 1476–1492, doi:10.1016/j.quascirev.2008.04.015.

Snowball, I., and P. Sandgren (2002), Geomagnetic field variations in northern Sweden during the Holocene quantified from varved lake sediments and their implications for cosmogenic nuclide production rates, *Holocene*, *12*, 517–530, doi:10.1191/0959683602hl562rp.

Snowball, I., L. Zillén, A. Ojala, T. Saarinen, and P. Sandgren (2007), FENNOSTACK and FENNORPIS: Varve dated Holocene palaeomagnetic secular variation and relative palaeointensity stacks for Fennoscandia, *Earth Planet. Sci. Lett.*, *255*, 106–116, doi:10.1016/j.epsl.2006.12.009.

Steele, M., and W. Ermold (2004), Salinity trends on the Siberian shelves, *Geophys. Res. Lett.*, *31*, L24308, doi:10.1029/2004GL021302.

Steele, M., J. Morison, W. Ermold, I. Rigor, M. Ortmeyer, and K. Shimada (2004), Circulation of summer Pacific halocline water in the Arctic Ocean, *J. Geophys. Res.*, *109*, C02027, doi:10.1029/2003JC002009.

Steele, M., W. Ermold, and J. Zhang (2008), Arctic Ocean surface warming trends over the past 100 years, *Geophys. Res. Lett.*, *35*, L02614, doi:10.1029/2007GL031651.

Stoner, J. S., and G. St-Onge (2007), Magnetic stratigraphy in paleoceanography: Reversals, excursions, paleointensity, and secular variation, in *Proxies in Late Cenozoic Paleoceanography*, edited by C. Hillaire-Marcel and A. de Vernal, pp. 99–138, doi:10.1016/S1572-5480(07)01008-1, Elsevier, Amsterdam.

Stoner, J. S., A. Jennings, G. B. Kristjánsdóttir, G. Dunhill, J. T. Andrews, and J. Hardardóttir (2007), A paleomagnetic approach toward refining Holocene radiocarbon-based chronologies: Paleoceanographic records from the north Iceland (MD99-2269) and east Greenland (MD99-2322) margins, *Paleoceanography*, *22*, PA1209, doi:10.1029/2006PA001285.

St-Onge, G., J. S. Stoner, and C. Hillaire-Marcel (2003), Holocene paleomagnetic records from the St. Lawrence Estuary, eastern Canada: Centennial- to millennial-scale geomagnetic modulation of cosmogenic isotopes, *Earth Planet. Sci. Lett.*, *209*, 113–130, doi:10.1016/S0012-821X(03)00079-7.

St-Onge, G., T. Mulder, D. J. W. Piper, C. Hillaire-Marcel, and J. S. Stoner (2004), Earthquake and flood-induced turbidites in the Saguenay Fjord (Québec): A Holocene paleoseismicity record, *Quat. Sci. Rev.*, *23*, 283–294, doi:10.1016/j.quascirev.2003.03.001.

Stroeve, J., M. Serreze, S. Drobot, S. Gearheard, M. Holland, J. Maslanik, W. Meier, and T. Scambos (2008), Arctic sea ice extent plummets in 2007, *Eos Trans. AGU*, *89*(2), 13, doi:10.1029/2008EO020001.

Thompson, D. W. J., and J. M. Wallace (1998), The Arctic Oscillation signature in the wintertime geopotential height and temperature fields, *Geophys. Res. Lett.*, *25*, 1297–1300, doi:10.1029/98GL00950.

Vare, L. L., G. Massé, T. R. Gregory, C. W. Smart, and S. T. Belt (2009), Sea ice variations in the central Canadian Arctic Archipelago during the Holocene, *Quat. Sci. Rev.*, *28*, 1354–1366, doi:10.1016/j.quascirev.2009.01.013.

Vavrus, S., and S. P. Harrison (2003), The impact of sea-ice dynamics on the Arctic climate system, *Clim. Dyn.*, *20*, 741–757.

Venegas, S. A., and L. A. Mysak (2000), Is there a dominant timescale of natural climate variability in the Arctic?, *J. Clim.*, *13*, 3412–3434, doi:10.1175/1520-0442(2000)013<3412:ITADTO>2.0.CO;2.

Verosub, K. L., P. J. Mehringer Jr., and P. Waterstraat (1986), Holocene secular variation in western North America: Paleomagnetic record from Fish Lake, Harney County, Oregon, *J. Geophys. Res.*, *91*, 3609–3624, doi:10.1029/JB091iB03p03609.

Weeks, R., C. Laj, L. Endignoux, M. Fuller, A. Roberts, R. Manganne, E. Blanchard, and W. Goree (1993), Improvements in long-core measurement techniques: Applications in paleomagnetism and paleoceanography, *Geophys. J. Int.*, *114*, 651–662, doi:10.1111/j.1365-246X.1993.tb06994.x.

Zhang, X. D., M. Ikeda, and J. E. Walsh (2003), Arctic sea ice and freshwater changes driven by the atmospheric leading mode in a coupled sea ice-ocean model, *J. Clim.*, *16*, 2159–2177, doi:10.1175/2758.1.

Zijderveld, J. D. (1967), Demagnetization of rocks: Analysis of results, in *Methods in Paleomagnetism*, edited by D. W. Collinson, K. M. Creer, and S. K. Runcorn, pp. 254–286, Elsevier, Amsterdam.

F. Barletta, D. Ledu, A. Rochon, and G. St-Onge, ISMER, UQAR, 310 Allée des Ursulines, Rimouski, QC G5L 3A1, Canada. (francesco.barletta@uqar.qc.ca; david.ledu@uqar.qc.ca; andre_rochon@uqar.qc.ca; guillaume_st-onge@uqar.qc.ca)

A. de Vernal, GEOTOP, Université du Québec à Montréal, Montréal, QC H3C 3P8, Canada. (devernal.anne@uqam.ca)